THE JOURNAL OF BIOLOGICAL CHEMISTRY VOL. 287, NO. 39, pp. 32598–32616, September 21, 2012

Glycosphingolipids Are Essential for Intestinal Endocytic Function*

Received for publication, April 11, 2012, and in revised form, July 30, 2012 Published, JBC Papers in Press, July 31, 2012, DOI 10.1074/jbc.M112.371005

Richard Jennemann[‡1], Sylvia Kaden[‡], Roger Sandhoff[‡§], Viola Nordström[‡], Shijun Wang[‡], Martina Volz[‡], Sylvie Robine[¶], Nicole Amen[‡], Ulrike Rothermel[‡], Herbert Wiegandt[‡], and Hermann-Josef Gröne[‡2]

From the [‡]Department of Cellular and Molecular Pathology, German Cancer Research Center, 69120 Heidelberg, Germany, [§]Morphogenesis and Intracellular Signaling, Institut Curie-CNRS, 75248 Paris, France, and the [¶]Lipid Pathobiochemistry Group, German Cancer Research Center, 69120 Heidelberg, Germany

Background: The intestine contains high concentrations of glycosphingolipids, but their function remained unclear.
Results: In newborn mice lacking glycosphingolipids, intestinal epithelia were indistinguishable from control littermates. However, a few days after birth, severe defects in epithelial differentiation occurred.
Conclusion: Glycosphingolipid expression in the intestinal epithelium is quintessential for maintenance of resorptive function.
Significance: Glycosphingolipids are essential for enterocyte function but not for brush border formation.

Glycosphingolipids (GSLs) constitute major components of enterocytes and were hypothesized to be potentially important for intestinal epithelial polarization. The enzyme UDP-glucose ceramide glucosyltransferase (Ugcg) catalyzes the initial step of GSL biosynthesis. Newborn and adult mice with enterocyte-specific genetic deletion of the gene *Ugcg* were generated. In newborn mutants lacking GSLs at day P0, intestinal epithelia were indistinguishable from those in control littermates displaying an intact polarization with regular brush border. However, those mice were not consistently able to absorb nutritional lipids from milk. Between postnatal days 5 and 7, severe defects in intestinal epithelial differentiation occurred accompanied by impaired intestinal uptake of nutrients. Villi of mutant mice became stunted, and enterocytes lacked brush border. The defects observed in mutant mice caused diarrhea, malabsorption, and early death. In this study, we show that GSLs are essential for enterocyte resorptive function but are primarily not for polarization; GSLs are required for intracellular vesicular transport in resorption-active intestine.

The intestine is the principal organ for digestion and absorption of nutrients. In the small intestine, enterocytes (columnar epithelial cells) cover the surfaces of villi, which contain thousands of densely packed apical microvilli that further amplify the surface area for absorption of nutrients.

Glycosphingolipids (GSLs)[3] are major constituents of enterocytes (1). Because of their high enterocytic expression, GSLs might be involved in several cellular processes in polarized intestinal epithelia. It could be shown that GSLs are integral constituents of lipid microdomains that seem to play important roles in membrane organization (2) and in endocytosis (3) of nutrients. In addition, GSLs might influence the biosynthesis (4) and intracellular transport of proteins (5). GSLs have been described to influence membrane receptors such as the insulin and EGF receptor (6–9).

The structural relevance of GSL synthesis in the intestine could be demonstrated in *Caenorhabditis elegans* mutants with significantly decreased glucosylceramide-based GSLs. Worms devoid of GSLs showed a pronounced growth arrest. The defect could be revoked by reexpression of glucosylceramide synthase in the digestive tract (10). This study highlighted the importance of intestinal GSLs, whereas GSL expression, different from the mouse, was dispensable for other tissues, including neuronal cells (10). In addition, a recent report suggested that GSLs were pivotal for epithelial polarization in *C. elegans.* With a marked reduction of GSL synthesis, worms developed multiple ectopic lumens in their intestine and showed degraded microvilli (11).

To dissect the role of GSLs for intestinal function in mammals, we used a novel mouse model in which GSL biosynthesis was genetically deleted in an enterocyte-specific manner by elimination of the gene *Ugcg* (glucosylceramide synthase), which encodes the key enzyme of the GSL biosynthesis pathway for all GSLs produced by enterocytes. To achieve specific deletion of GSLs in enterocytes, mice with the loxP-flanked *Ugcg* gene (12) were mated with mice expressing Cre recombinase under control of the villin promoter (13). As villin expression starts early with the developing intestine at embryonic day E10 and is then ubiquitously distributed throughout the small intestine at embryonal days E14 to E15 (14), our model was also especially suited to investigate the consequences of *Ugcg* deletion in newborn mice. A second model was employed in which GSLs were deleted specifically in enterocytes during adulthood, again under control of the villin promoter (15).

Complete genetic deletion of GSLs in the intestinal epithelium was achieved in both models. Although GSLs were absent

* This work was supported by Deutsche Forschungsgemeinschaft Grants-in-aid SFB 938 and GK 880 (to H.-J. G.).
[1] To whom correspondence may be addressed: Cellular and Molecular Pathology, German Cancer Research Center, Im Neuenheimer Feld 280, 69120 Heidelberg, Germany. Tel.: 49-6421-424356; Fax: 49-6421-424352; E-mail: r.jennemann@dkfz.de.
[2] To whom correspondence may be addressed: Cellular and Molecular Pathology, German Cancer Research Center, Im Neuenheimer Feld 280, 69120 Heidelberg, Germany. Tel.: 49-6421-424350; Fax: 49-6421-424352; E-mail: h.-j.groene@dkfz.de.
[3] The abbreviations used are: GSL, glycosphingolipid; NBD, 12-(*N*-methyl-*N*-(7-nitrobenz-2-oxa-1,3-diazol-4-yl)); DCE, dichloroethane; SM, sphingomyelin; EDU, 5-ethynyl-2′-deoxyuridine.

in enterocytes of newborn mutant mice at postnatal day P0, the epithelial brush border had been formed regularly. However, the ability to absorb lipids from milk was already significantly reduced at P0. A few days after birth, GSL deletion in enterocytes caused severe structural defects of the epithelium accompanied by loss of the brush border. The lack of nutrient absorption led to the early death of mice.

This study has now demonstrated that glycosphingolipids are initially not required for intestinal epithelial polarization, but they are quintessential for proper intestinal function, namely endocytic uptake of nutrients, in particular lipids, when intestine starts its activity after birth.

EXPERIMENTAL PROCEDURES

Mice—Mice with loxP-flanked *Ugcg* gene (*Ugcg* f/f) were generated and genotyped by PCR and Southern blot analysis as described previously (12). Cell-specific *Ugcg*-deficient newborn mice were generated by crossing *Ugcg* f/f mice with animals expressing cre recombinase constitutively (VilCre, The Jackson Laboratory, Bar Harbor, ME) (13). To investigate the consequences of the Ugcg deletion during adulthood, an inducible model was developed by crossing *Ugcg* f/f mice with tamoxifen-inducible VilCreERT2 animals (15). Mice were genotyped as described previously (13, 15). Resulting heterozygous mice (*Ugcg* f/+/VilCre or *Ugcg* f/+/VilCreERT2) were bred again with *Ugcg* f/f mice, and 25% of the offspring, reflecting normal Mendelian inheritance, carried the homozygous genetic deletion of *Ugcg* (*Ugcg* f/f/VilCre and *Ugcg* f/f/VilCreERT2). Corresponding heterozygous (*Ugcg* f/+/VilCre and *Ugcg* f/+/VilCreERT2) as well as "wild type" litters (*Ugcg* f/+/and *Ugcg* f/f) showed no obvious phenotype and were used as controls. *Ugcg* gene deletion in adult *Ugcg* f/f/VilCreERT2 mice was initiated by intraperitoneal application of 1 mg of tamoxifen in 100 μl of sunflower seed oil (both, Sigma) for 3 consecutive days. Respective controls were treated in parallel with tamoxifen. All animal experiments were approved by federal law.

LacZ Staining to Evaluate Cre Expression—LacZ-Rosa26 reporter mice (kindly provided by G. Schütz, DKFZ-Heidelberg) bearing a β-galactosidase gene were crossed with mice expressing the VilCre transgene. In the resulting offspring bearing both LacZ and cre, β-galactosidase activity was measured as described previously (15).

Sphingolipid and Phospholipid Analysis—Freshly dissected tissue ~2 cm in length was frozen in liquid nitrogen and lyophilized. Tissues were powdered, and dry weight was determined. Lyophilized samples were extracted with 2 ml of $CHCl_3$/CH_3OH/H_2O, 10:10:1, v/v, under sonication in a water bath at 50 °C for 15 min. Supernatants were collected after centrifugation at 4000 rpm for 10 min. The pellets were again extracted with 2 ml of $CHCl_3$/CH_3OH/H_2O, 10:10:1 (v/v), and thereafter with $CHCl_3$/CH_3OH/H_2O, 30:60:8 (v/v), as described above. All supernatants were combined and dried under a stream of nitrogen. For the determination of phospholipids, aliquots from the crude intestinal extracts corresponding to 0.05 mg of dry tissue were loaded on thin layer chromatography (TLC) plates (Merck). TLC plates were developed in running solvent $CHCl_3$/CH_3OH/H_2O, 65:25:4 (v/v), and phospholipids were visualized with copper reagent (10% $CuSO_4$ in 8% H_3PO_4) at 180 °C for 5–10 min. For determination of GSLs, sphingomyelin, and ceramide, the crude intestinal extracts were treated with 1 ml of 0.1 M KOH in CH_3OH at 50 °C for 4 h to eliminate phospholipids and triglycerides. Samples were neutralized with acetic acid and dried. Potassium acetate was removed using reversed phase column chromatography (RP18). For this purpose, small glass pipettes were filled with 200 μl of RP18 material (Waters Associates, Milford, MA) and preconditioned with 2 ml each of methanol, H_2O, and 0.1 M KAc in H_2O. The samples were suspended in 1 ml of H_2O and applied to the columns; the reagent tubes were washed two times with 0.1 M Kac, which was then also loaded. Columns were washed with 4 ml of H_2O, and sphingolipids were eluted with 4 ml of methanol and dried. For quantification of sphingomyelin, aliquots from the saponified samples corresponding to 0.05 mg of dry tissue were spotted on TLC plates. TLC plates were developed and stained as described above for phospholipids. Amounts corresponding to 0.25 mg of dry tissue were spotted on TLC plates for determination of ceramides. Running solvent was $CHCl_3$/CH_3OH/HAc, 190:9:1, v/v. Visualization of ceramides with copper reagent was performed as described above. Glycosphingolipids were separated into neutral and acidic (sialic acid-containing) components by ion exchange chromatography. Glass pipettes were filled with 200 μl of DEAE-Sephadex A25 (GE Healthcare), and columns were preconditioned with 2 ml of methanol. The samples were solved in 2 ml of methanol and applied to the columns. Reagent tubes were rinsed two times with 1 ml of methanol, and neutral GSLs were completely eluted from the columns with additional 2 ml of methanol. Acidic GSLs were then eluted with 2 ml of 0.5 M KAc in CH_3OH. Acidic GSLs were dried and solved in 5 ml of H_2O and desalted via preconditioned RP18 columns as described above. Neutral GSLs were thoroughly dried and kept for several hours in a vacuum desiccator. GSLs were solved in 200 μl of dichloroethane (DCE) and acetylated by the addition of 50 μl of acetic anhydride and 50 μl of 0.1% dimethylaminopyridine in DCE at 37 °C for 1 h. The solvents were evaporated under a N_2 stream by addition of 200 μl of toluene, respectively, three times. Glass pipettes were filled with 400 μl of Florisil (Merck) and washed with 4 ml of DCE/*n*-hexane, 4:1, v/v. The acetylated neutral GSLs were solved in the same solvent mixture and applied to the columns followed by washing steps with DCE/*n*-hexane, 4:1, and DCE, 4 ml each. Neutral GSLs were eluted from Florisil columns with 4 ml of DCE/acetone, 1:1 (v/v), and dried. To remove acetyl groups from sugar moieties, neutral GSLs were solved in 0.1 M KOH in methanol and incubated at 37 °C for 2 h. After neutralization with acetic acid, the purified neutral GSLs were dried

TABLE 1
UPLC gradient elution of sphingolipids for tandem-mass spectrometry detection

Time	Flow rate	Solvent A	Solvent B	Slope
min	*ml/min*	*%*	*%*	
Initial	0.45	100	0	Initial
0.1	0.45	100	0	Linear
0.2	0.45	92	8	Linear
5.0	0.45	20	80	7
5.75	0.45	20	80	Linear
6.00	0.45	100	0	Linear
7.00	0.45	100	0	Linear

TABLE 2
Antibodies used for immunofluorescence
The following abbreviations are used: *d,* donkey; *g,* goat; *m,* mouse; *rb,* rabbit.

1st antibody	Host	Dilution	Supplier	2nd antibody	Host	Dilution	Supplier
1. GM1[a]	rb	1:20	Matreya	Anti-rb IgG AF488	d	1:200	Invitrogen
2. Villin	g	1:5	Santa Cruz Biotechnology	Anti-g IgG AF546	d	1:200	Invitrogen
1. GM1[a]	m	1:10	Seikagaku	Anti-m IgM AF488	g	1:200	Invitrogen
2. Clathrin	rb	1:100	Millipore	Anti-rb IgG AF546	d	1:200	Invitrogen
1. Rab11[a]	m	1:20	Millipore	Anti-m IgG AF488	d	1:500	Invitrogen
2. GM1	rb	1:20	Matreya	Anti-rb IgG AF546	d	1:200	Invitrogen
1. E-cadherin[b]	m	1:25	BD Biosciences	Anti-m IgG AF488	d	1:200	Invitrogen
2. Villin	g	1:5	Santa Cruz Biotechnology	Anti-g IgG AF546	d	1:200	Invitrogen
1. β-Catenin[b]	m	1:20	BD Biosciences	Anti-m IgG AF488	d	1:200	Invitrogen
2. Villin	g	1:5	Santa Cruz Biotechnology	Anti-g IgG AF546	d	1:200	Invitrogen
Lamp1[a]	rb	1:50	Acris	Anti-rb IgG AF488	d	1:200	Invitrogen

[a] Staining on frozen sections.
[b] Staining on paraffin sections.

TABLE 3
Antibodies used for immune electron microscopy
The following abbreviations are used: *g,* goat; *m,* mouse; *rb,* rabbit; frozen sections.

1st antibody	Host	Dilution	Supplier	2nd antibody	Host	Dilution	Supplier
GA1	rb	1:100	Acris	Protein A gold 10 nm		1:70	CMC
GM1	rb	1:20	Matreya	Protein A gold 10 nm		1:70	CMC
1. GM1	m	1:20	Seikagaku	Anti-m IgG/M 10 nm gold	g	1:30	Aurion
2. Clathrin	rb	1:300	Millipore	Protein A gold 5 nm		1:80	CMC
1. Rab11	m	1:10	Millipore	Anti-m IgG/M 10 nm gold	g	1:30	Aurion
2. GM1	rb	1:20	Matreya	Protein A gold 5 nm		1:80	CMC

down and desalted by RP18 column chromatography as described above. An amount corresponding to 0.25 mg of dry intestine was loaded on TLC plates for the staining of neutral and acidic GSLs. Running solvent for neutral GSLs was $CHCl_3$/CH_3OH/H_2O, 62.5:30:6, v/v; and $CHCl_3$/CH_3OH, 0.2% $CaCl_2$, 60:35:8 (v/v), was used for acidic GSLs. TLC plates were sprayed with 0.2% orcinol in 10% sulfuric acid at 120 °C for ~10 min to visualize GSLs.

Quantification of Fatty Acids and Cholesterol in Stool—1 cm of the distal rectum of sacrificed mice (controls, $n = 8$, and *Ugcg* f/f/VilCre, $n = 6$) was resected and the feces content carefully removed with a small forceps. Isolated stools were freeze-dried, and the dry weight was determined and extracted essentially as described previously (16). Lipids were quantified using a Shimadzu CS-9310PC TLC scanner (Shimadzu Europe, Duisburg, Germany) at a wavelength of 580 nm.

LC-MS/MS Quantification of Ceramides and Hexosylceramides (GlcCer)—Aliquots of the above obtained, saponified, and desalted lipid extracts corresponding to 25 μg of tissue dry weight were dissolved in 1 ml of 95% methanol containing a mixture of internal sphingolipid standards for LC-MS/MS analysis. Among these were the glucosylceramides GlcCer(d18:1;14:0), GlcCer(d18:1;19:0), GlcCer(d18:1;25:0), and GlcCer(d18:1;31:0), each in an amount of 2 pmol, as well as the ceramides Cer(d18:1;14:0), Cer(d18:1;19:0), Cer(d18:1;25:0), Cer(d18:1;31:0), and Cer(t18:0;14:0), each in an amount of 4 pmol. LC-MS/MS analysis was performed on a Xevo TQ-S tandem mass spectrometer coupled to an automated Acquity I class UPLC system using a ACQUITY UPLC® BEH C18 1.7 μm column (length 50 mm, diameter 2.1 mm) all from Waters Corp. The column was equilibrated in buffer A (95% methanol, 0.05% formic acid, and 1 mM ammonium acetate), and lipids were eluted with increasing percent of buffer B (99% 2-propanol, 1% methanol, 0,05% formic acid, and 1 mM ammonium acetate) at a flow rate of 0.45 ml/min (gradient see Table 1).

TABLE 4
Primary antibodies used for Western blot
The following abbreviations are used: g, goat; m, mouse; rb, rabbit; 2nd antibody, g anti-m or g anti-rb IgG, 1:1000, Santa Cruz Biotechnology.

1st antibody	Host	Dilution	Supplier
Caveolin-1	m	1:1000	BD Biosciences
Clathrin	rb	1:100	Santa Cruz Biotechnology
Rab4	rb	1:500	GeneTex
Rab5	rb	1:200	Santa Cruz Biotechnology
Rab11	m	1:1000	BD Biosciences
β-Catenin	m	1:2000	BD Biosciences
E-cadherin	m	1:3000	BD Biosciences
Lc3	rb	1:1000	Sigma
β-Actin	rb	1:500	Santa Cruz Biotechnology

Sphingolipids were detected in selected reaction monitoring mode with their respective transitions. The decision basis for the incorporation of individual sphingolipids into the final selected reaction monitoring list was based on nanospray direct infusion in precursor ion scan m/z +264 mode identifying ceramides and hexosylceramides containing either a d18:1 or a t18:0 sphingoid base. For quantification, peak areas of individual lipid species were divided by the respective average internal standard area, multiplied by the amount of this internal standard, and finally divided by the tissue dry weight used. With the internal ceramide standards Cer(d18:1;31:0) and Cer(t18:0;31:0), an average response factor of 12.2 ± 1.8 for the sensitivity of sphingosine species over phytosphingosine species was determined and taken into account to quantify the phytosphingosine-containing ceramides and hexosylceramides.

Isolation of Milk Sugars from Feces and TLC—Feces were extracted essentially as described previously (16). An aliquot of the crude extract was directly loaded on a TLC plate and developed in running solvent pyridine/ethyl acetate/glacial acetic acid/water 5:5:1:3 by volume. Visualization with orcinol reagent was performed as described above.

Measurement of Intestinal Sialidase Activity—Homogenates of total small intestines of mutant and control ($n = 4$ each) were

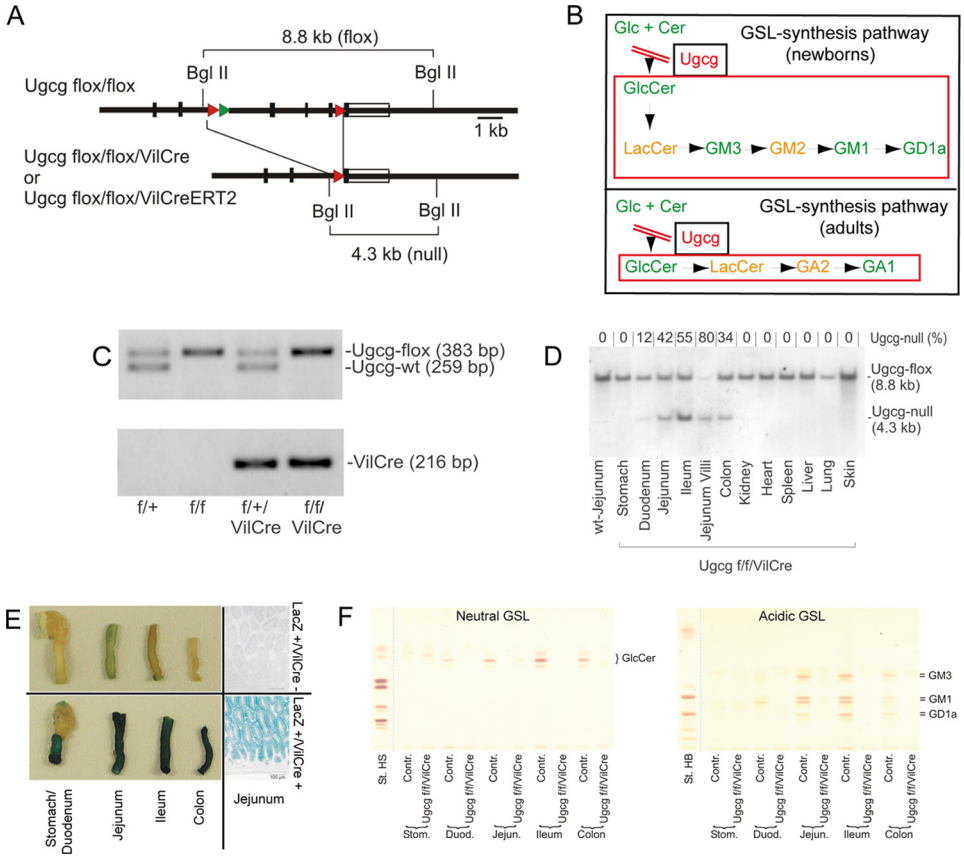

FIGURE 1. ***Ugcg* cloning strategy, GSL synthesis pathway, genotyping, and cre activity determination.** *A, Ugcg* gene deletion was initiated by generating mice expressing loxP-flanked *Ugcg* alleles together with cre recombinase under the villin promoter. *B,* GSL synthesis pathway in newborn and adult mice. The *red boxes* show GSLs expected to be absent in *Ugcg* f/f/VilCre mice. *Yellow* labeled GSLs LacCer and GM2 in newborns as well as LacCer and GA2 in adult mice intestine represent intermediates that are immediately used to synthesize higher GSL products; for nomenclature of GSL, see Ref. 24. *C,* mutant mice were genotyped by PCR, and *Ugcg* gene deletion could be confirmed by Southern blot analysis (*D*, values from densitometry on top). *E,* cre activity in the intestine has been indicated by a *dark blue* staining in mice expressing the villin-cre transgene in combination with a *lacZ* reporter gene throughout the whole intestine. The stomach tested negative. *F,* GSL analysis of intestinal compartments of *Ugcg* f/f/VilCre mice confirmed the results obtained by *lacZ* staining and Southern blot. Glycosphingolipids were depleted throughout the whole intestinal epithelium. *Contr.*, control.

mixed with siallyllactose (Sigma,) and the digest was performed at 37 °C either for 30 min or in a time-dependent manner essentially as described previously (17). The cleavage product lactose was quantified by densitometry.

Fatty Acid/Glucose Uptake—Animals 3–4 days and 6–7 days after birth (controls, $n = 12$, and *Ugcg* f/f/VilCre, $n = 9$) were anesthetized with isoflurane. The peritoneum was opened, and a 1-cm part of the intestinal jejunum of the same area was ligated. 100 μl of a solution containing 10 μM fluorescent-labeled stearic acid (NBD-stearic acid, Avanti Polar Lipids, Alabaster, AL) and 20 μM fatty acid-free BSA (Sigma) in PBS was injected, and uptake was performed for 10 min in the dark. For investigation of glucose uptake studies, 60 μM 2-NBD-glucose (Invitrogen) in PBS was used. The ligated part of the jejunum was resected, washed with pre-warmed PBS, and immediately frozen in liquid nitrogen. Cryosections of 5 μM thickness were air-dried for 30 min in the dark, embedded in Fluoromount G (Southern Biotech, Birmingham, AL) for detection of NBD-stearic acid or Vitro-Clud® (Langenbrink, Emmendingen, Germany) for NBD-glucose staining, and scanned with a confocal laser microscope (TCS-SL, Leica, Wetzlar, Germany).

Liposome Preparation and Uptake—To investigate whether GSL depletion influenced the absorption of fat in macroscale amounts, liposomes were prepared for this uptake approach. Each lipid, *i.e.* cholesterol, phosphatidylcholine, and triolein, was solved at a concentration of 10 mg/ml in $CHCl_3/CH_3OH$, 2:1 (v/v). Fluorescent NBD-stearic acid (Avanti Polar Lipids, Alabaster, AL) was solved in $CHCl_3$ at a concentration of 1 mg/ml. For the preparation of liposomes, 160 μl of triolein, and 20 μl of cholesterol, phosphatidylcholine, and NBD stearic acid each were mixed and dried under a stream of nitrogen. The lipid mixture was subsequently dried in a vacuum desiccator for 30 min. After addition of 500 μl of PBS, liposomes were formed by incubation of the mixture in an ultrasound water bath at 50 °C for 15 min. For uptake studies of liposomes, mice were anesthetized, and a 2-cm part of the jejunum ~4 cm caudally from the duodenum was ligated with clamps. 100 μl of the liposome solution was injected (controls, $n = 8$; *Ugcg* f/f/VilCreERT2, $n = 3$). The liposome containing jejunum was excised after 15 min, rinsed with 5 ml of PBS, and immediately frozen on dry ice in O.C.T. Tissue-Tek embedding medium (Sukura Finetek, Alphen aan den Rijn, The Netherlands). Sections of 5 μm were mounted with fluorescent mounting medium (DAKO, Hamburg, Germany) containing 1:2000 diluted DRAQ5 (Alexis, Shepshed, UK) for nuclear staining and scanned with a confocal laser microscope (TCS-SL, Leica, Wetzlar, Germany).

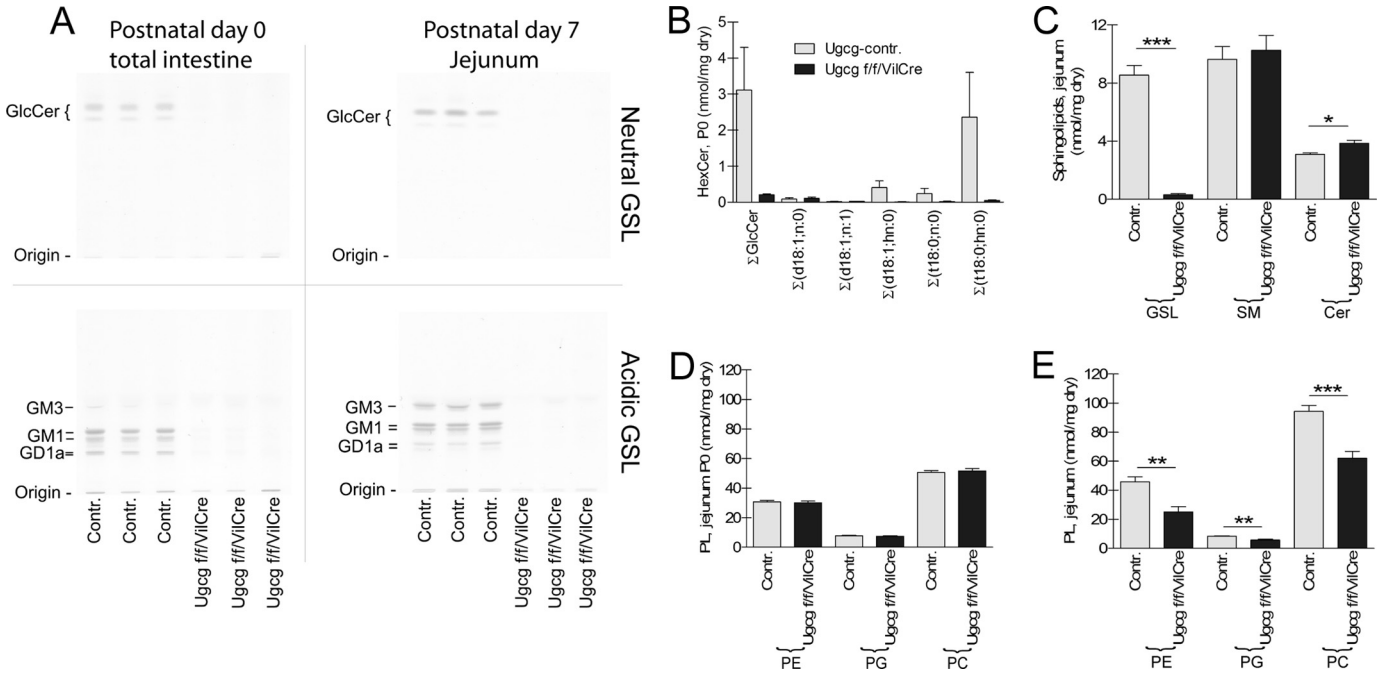

FIGURE 2. **Sphingolipid analysis.** *A,* GSLs as synthesis products of Ugcg were depleted in mutant tissue already in newborn mice at day P0. *B,* as revealed by mass spectrometry, the total GlcCer depletion rate in newborn *Ugcg* f/f/VilCre mice at P0 was >90% (controls (*Contr.*) and mutant, $n = 3$, respectively). A minor GlcCer fraction with sphingosine and nonhydroxylated fatty acids in its ceramide anchor was not affected by the *Ugcg*-gene deletion and might likely be originated from cells in which the cre recombinase was not active. *C,* sphingomyelin in mutant intestine had a similar concentration as in control tissue, and ceramide content increased slightly in *Ugcg* f/f/VilCre intestine as compared with controls. *D,* phospholipid content was not altered in newborn *Ugcg* f/f/VilCre mice at P0 ($n = 4$, respectively). *E,* intestinal phospholipid concentrations significantly decreased in mutant tissue at P5 to P7 (*PE,* phosphatidylethanolamine; *PG,* phosphatidylglycerol; *PC,* phosphatidylcholine), controls and *Ugcg* f/f/VilCre, $n = 6$ each.

Light Microscopy and Immunohistochemistry—Light microscopy at different time points (controls, $n > 40$, and *Ugcg* f/f/VilCre, $n > 30$) and immunohistochemistry/immunofluorescence (controls, $n = 4$, and *Ugcg* f/f/VilCre, $n = 4$) were performed as described previously (12). Paraffin-embedded buffered paraformaldehyde (4%, pH 7.3)-fixed sections were stained by hematoxylin and eosin (H&E, Chroma, Köngen, Germany). Activity of alkaline phosphatase was determined by overlay of sections with alkaline phosphatase substrate solution. For immunohistochemistry of rat anti-mouse Ki67, 1:200 (DAKO, Hamburg, Germany), an alkaline phosphatase-anti-alkaline-phosphatase reaction was used (12). Goat anti-villin antibodies (Santa Cruz Biotechnology, Santa Cruz, CA) were diluted 1:20. A 1:300 diluted biotinylated anti-goat antibody was used as secondary antibody (Dianova, Hamburg, Germany), followed by a streptavidin-HRP complex (Vector SA-5004, Vector Laboratories, Burlington, CA) at a dilution of 1:200. All antibodies and dilutions used in immunofluorescence are listed in Table 2.

In Vivo DNA Labeling with EDU—Mice were injected intraperitoneally with 200 μg of EDU (Invitrogen). After 24 h, mice were sacrificed, and intestinal parts were embedded in paraffin. Sections of 5 μm thickness were taken, and EDU-labeled cells were stained by click reaction as described by Salic and Mitchison (18).

Electron Microscopy—Intestinal sections were fixed with a mixture of 0.05% ruthenium red (AppliChem, Darmstadt, Germany), 2.5% glutaraldehyde, and 0.2 M cacodylate buffer, pH 7.2 (both from Serva, Heidelberg, Germany), 1:1:1 (v/v) at room temperature for 2 h. Samples were washed three times with cacodylate buffer and fixed for a second time with 0.05% ruthenium red, 0.2 M cacodylate buffer, and 2% osmium tetroxide (Chempur, Karlsruhe, Germany), 1:1:1, by volume, at room temperature for 2 h. Samples were washed again with cacodylate buffer, dehydrated with a sequential ethanol gradient, and embedded in araldite (Serva, Heidelberg, Germany). Alternatively to ruthenium red, samples were fixed according to Karnovsky (19). Araldite-embedded tissue was cut (70 nm) and viewed in a transmission EM (Leo 910, Zeiss, Oberkochen, Germany).

Immune Electron Microscopy—Intestinal sections were prepared for cryoimmune-EM according to Tokuyasu *et al.* (20) to ensure that GSLs neither were extracted nor delocalized within the tissue. Sections of ~2–3 mm in length were immersion-fixed with 4% paraformaldehyde in PBS for 2 h. Subsequently, sections were allowed to sediment overnight in 2.3 M sucrose and have thereafter been frozen until use. Frozen ultrathin sections were obtained using an ultracut (UC6, Leica, Nussloch, Germany) and were placed on carbon-coated EM grids. The sections were blocked and labeled with antibodies as described previously (20). Primary antibodies and gold-labeled secondary antibodies or protein A gold are listed in Table 3. All primary antibodies were incubated at 4 °C overnight. Gold-labeled secondary antibodies or protein A were incubated at room temperature for 2 h. Images of labeled sections were taken using a transmission EM (Leo 910, Zeiss, Oberkochen, Germany).

Nile Red Staining for Lipids—For the staining of cryosections at P0, newborn mice were sacrificed after initial suckling ~2–4 h after birth, and one part of the intestinal jejunum with visible

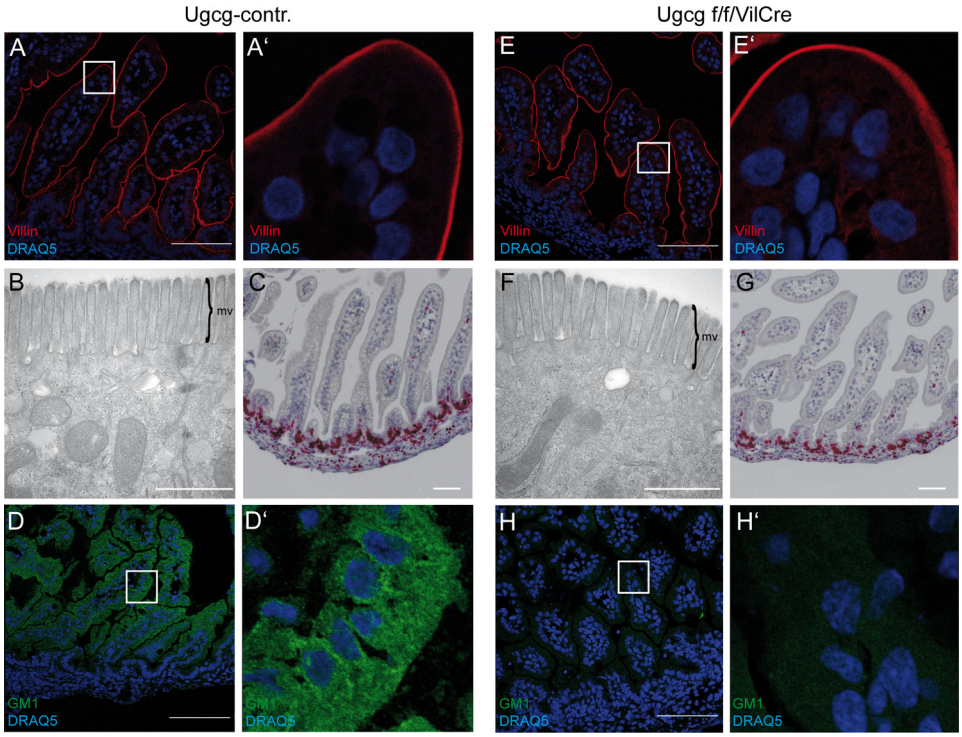

FIGURE 3. **Newborn *Ugcg* f/f/VilCre mice, although depleted of GSLs, show no conspicuous phenotype at P0.** (*A, A′, E,* and *E′*) The brush border marker protein villin was expressed in wild type and mutant mice at postnatal day P0. *B* and *F,* presence of an intact brush border could be confirmed by electron microscopy. *C* and *G,* as shown by anti-Ki67, no differences in proliferation were apparent between control and mutant mice. *D* and *D′*, GSL GM1 was found ubiquitously distributed in vesicle-like structures within the cytosol of enterocytes. *H* and *H′*, *Ugcg* f/f VilCre intestine stained negative for GM1. *Scale bars,* light microscopy, 100 μm; EM, 1 μm. *Contr.*, control.

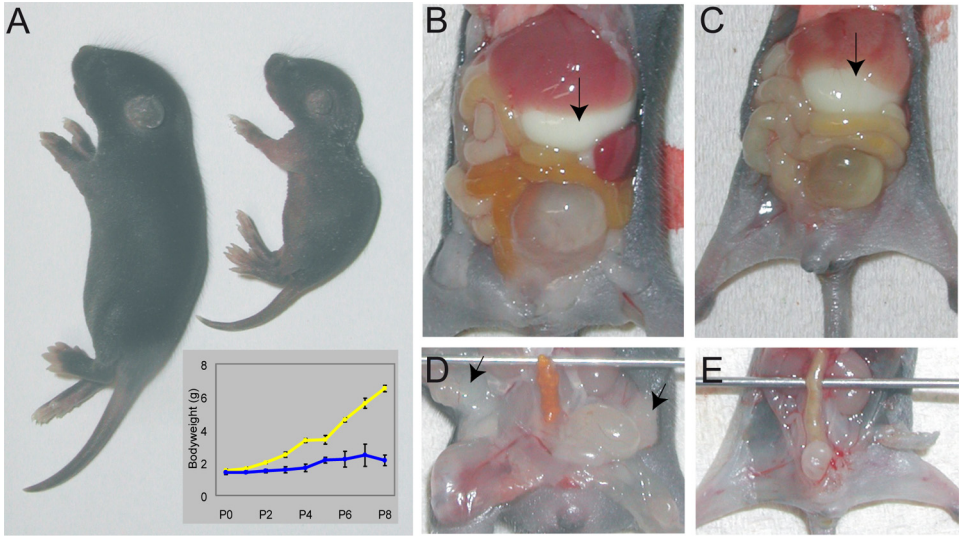

FIGURE 4. ***Ugcg*-deficient mice showed retarded postnatal weight gain and loss of body fat deposits.** *A, Ugcg* f/f/VilCre mice were of smaller size and displayed insignificant gain of weight (*A, inset*). *B* and *C,* control mice (*B*) and mutant mice (*C*) contained milk in their stomachs (*arrows*) 1 week after birth demonstrating successful suckling. *D* and *E,* gonadal fat deposits observed in controls (*D, arrows*) were not observed in mutant mice (*E*). Stools in the rectum of mutant mice appeared soft and still displayed milk-like color.

nutrient content was shortly perfused with 2 ml of ice-cold PBS and immediately frozen in Tissue-Tek embedding medium. Similarly, also one part of the jejunum was prepared from newborns at P7. 0.05% Nile red was dissolved in acetone. 10 μl of the stock solution was diluted 1:200 in glycerol/H_2O, 3:1 (v/v). 5-μm cryosections were covered with Nile red solution and scanned with a confocal laser microscope (TCS-SL, Leica, Wetzlar, Germany).

Western Blotting—Proteins were isolated from freshly prepared small intestine from the jejunum essentially as described elsewhere (21). Antibodies used are listed in Table 4.

mRNA Isolation and Quantitative RT-PCR—One ~1-cm piece of the intestinal jejunum was prepared from sacrificed animals. Adhering tissue was removed. Total mRNA was extracted as described previously (22). Quantitative real time RT-PCR was done using the LC-fast DNA Master SYBR Green

I kit PCR for the LightCycler (Roche Applied Science) as described previously (12), and mouse 18 S ribosomal RNA was used as reference (controls, $n = 8$, and *Ugcg* f/f/VilCre, $n = 8$).

Lipase Assay—Feces of newborn control ($n = 7$) and *Ugcg* f/f/VilCre ($n = 6$) mice were collected from rectums at day P6 and immediately frozen and stored at −80 °C until analysis. Feces were weighed and diluted 1:20 (w/v) with distilled water and dispersed. The suspension was centrifuged at 12,000 rpm and at 4 °C for 10 min. 5 μl of the respective supernatants were used for lipase assay. The assay was performed according to Ma *et al*. (23).

Determination of Triglycerides in Plasma—Triglycerides were measured with a triglyceride quantification kit (BioVision, Mountain View, CA) according to the manufacturer's recommendations (controls, $n = 11$; *Ugcg* f/f/VilCre, $n = 8$).

Statistics—Data were analyzed using Student's two-tailed unpaired *t* test. In all graphs, the mean values ± S.E. are shown. Significances are as follows: *, $p < 0.05$; **, $p < 0.01$; ***, $p < 0.001$.

RESULTS

Ugcg f/f/VilCre Mice Lack GSLs in the Intestine of Newborn Mice—To investigate the role of GSLs for intestinal function, mice were generated in which the *Ugcg* gene, encoding the key enzyme Ugcg involved in the initial step of the glucosylceramide based GSL synthesis pathway, was deleted in a cell-specific manner in enterocytes by using a villin-cre recombinase transgene (Fig. 1*A*). Deletion of Ugcg can be expected to result in absence of GSLs in the epithelium of the intestine in newborn and adult mice (Fig. 1*B*). A product of 383 bp indicated the floxed *Ugcg* allele and a fragment of 216 bp was indicative for the villin-cre transgene (Fig. 1*C*). As shown by Southern blot analysis, *Ugcg* gene deletion was restricted to the intestine (Fig. 1*D*). The specificity of the *Ugcg* gene deletion for the complete intestinal tract but not for the stomach was indicated by a LacZ staining (Fig. 1*E*). Consequently, all investigated intestinal parts of mutant mice showed GSL depletion (Fig. 1*F*). In agreement with the *Ugcg* gene deletion, depletion of glucosylceramide (GlcCer) and its further synthesis products, *e.g.* ganglioside GM1 and GD1a (24), was seen in newborn mice at P0 and P7 (Fig. 2*A*). The TLC data could be confirmed by LC-MS/MS. In our analysis from intestinal tissue at day P0, we could demonstrate that GlcCers with phytosphingosine- and α-hydroxylated fatty acid in their lipid anchor were by far the most prominent occurring species in the intestine (Fig. 2*B*). Those species of GlcCers were 40-fold reduced in mutant intestine of newborn mice at P0 (Fig. 2*B*). However, one minor GlcCer species with sphingosine and nonhydroxylated fatty acids, representing less than 5% of the total GlcCers, appeared unaltered in intestinal GSL extracts (Fig. 2*B*). These GlcCers may have originated from cells not affected by the Ugcg deletion such as muscle, endothelial, stroma, and goblet cells. Also, the possibility that the remnant was not GlcCer but GalCer cannot be excluded. The total sphingomyelin content in mutant intestine appeared almost unaltered (Fig. 2*C*), and ceramide increased ~20% in mutant tissue at P7 (Fig. 2*C*). The phospholipid concentration in intestinal extracts

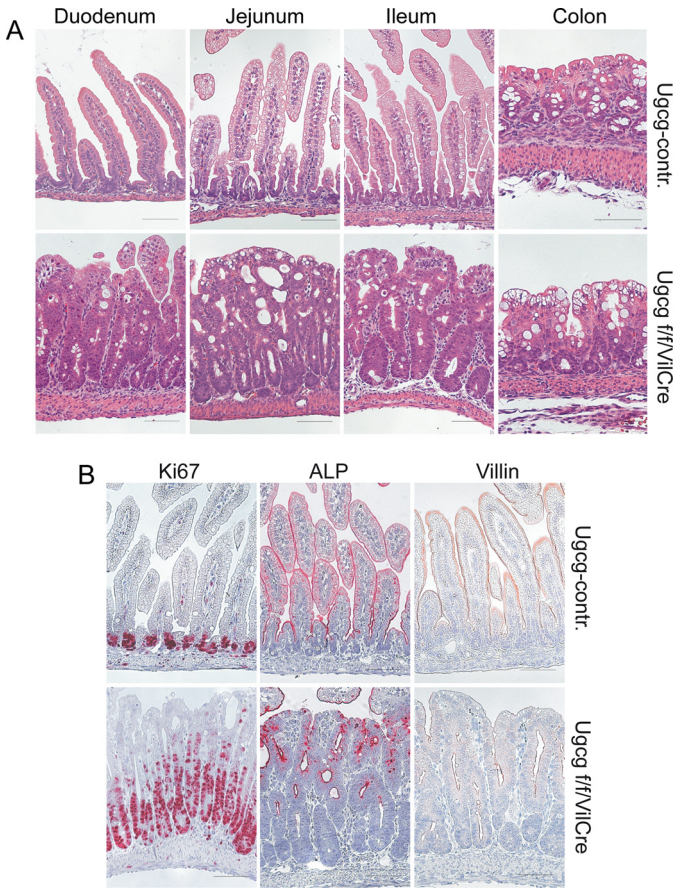

FIGURE 5. ***Ugcg* f/f/VilCre mice exhibited major structural defects in the intestine and impaired distribution of intestinal proteins 1 week after birth.** *A,* H&E staining of intestinal segments was as indicated. Pronounced structural defects were recognized in the mucosa of the small intestine of mutant mice with loss of villi and flattening of the mucosa as well as increased epithelial vacuolization. *B,* immunohistochemistry of polarization and proliferation marker of newborn mice at postnatal day P7. As exemplarily shown for sections of the jejunum, intestine from *Ugcg*-deficient mice displayed high levels of cell proliferation (*Ki67*). Mutant mice showed a patchy distribution of alkaline phosphatase expression (*ALP*) and almost a complete absence of the structural protein villin, both of which were present in the microvillar region of intact intestinal mucosa in control mice; *scale bars,* 100 μm. *Contr.*, control.

was not changed in newborn mice at P0 (Fig. 2*D*), but they significantly decreased in mutant intestines 5–7 days after birth (Fig. 2*E*). The intestinal cholesterol concentrations were slightly but not significantly reduced in mutant jejunum at P7 (*i.e. Ugcg* control, 22.5 ± 1.1 nmol/mg dry weight; *Ugcg* f/f/VilCre, 20.0 ± 1.9 nmol/mg dry weight).

Newborn Ugcg f/f/VilCre Mice at P0 Displayed Inconspicuous Morphology and Behavior—Although newborn mice lacked enterocytic GSLs at P0 (Fig. 2*A*), they and enterocytes were indistinguishable from their littermates in size and behavior. Expression of villin, required for correct alignment of the microvillar actin core bundle to anchor the brush border, was normal in mutants at P0, implying a regular polarization of the epithelium (Fig. 3, *A* and *E*, anti-villin immunofluorescence). The ultrastructure of intestinal epithelium was similar in mutants and controls (Fig. 3, *B* and *F*, electron micrographs). An increased proliferative property of the epithelium due to the absence of GSLs was not observed at P0 (Fig. 3, *C* and *G*). GSLs could be detected equally distributed in vesicular like dots

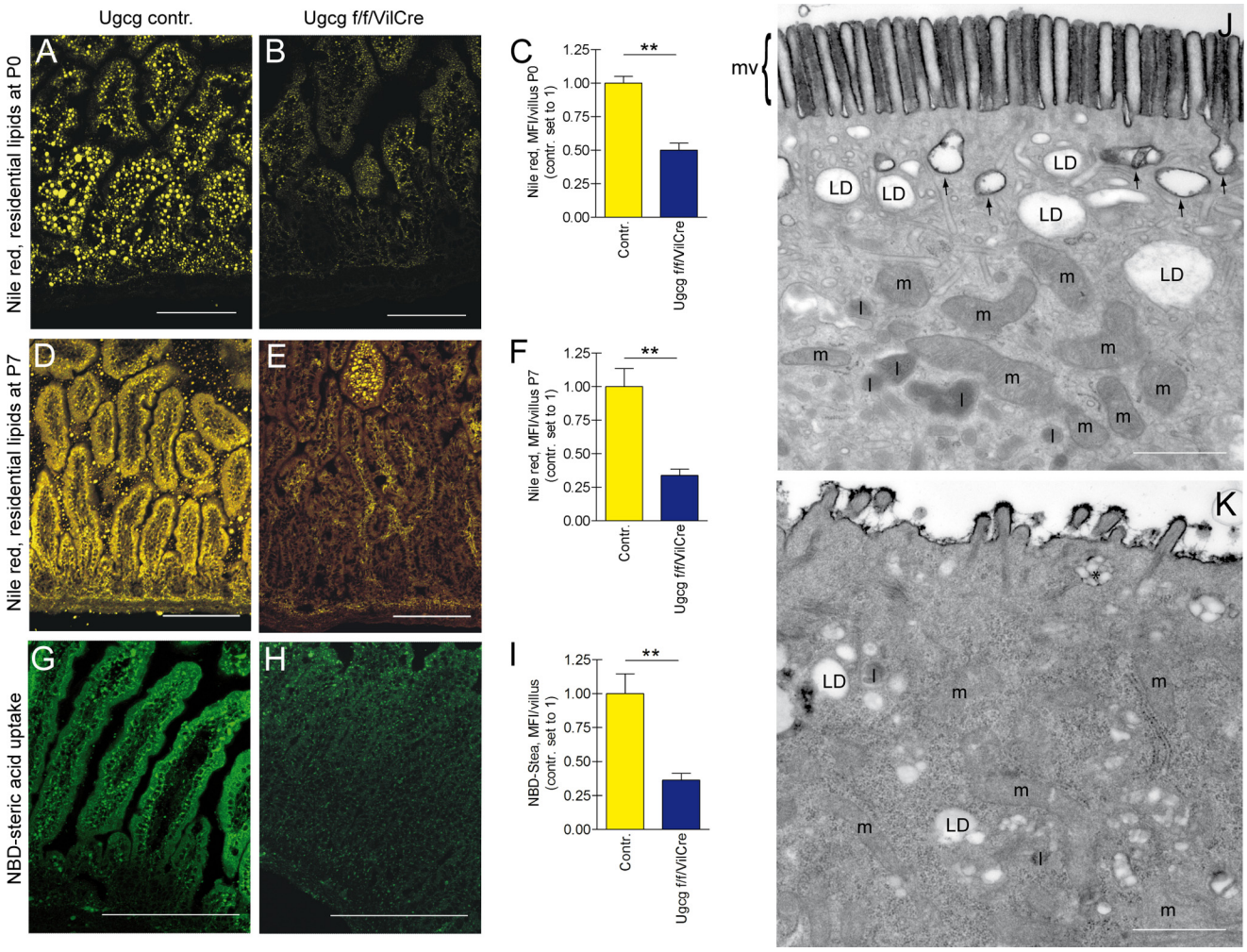

FIGURE 6. **Mice lacking glycosphingolipids in the intestine showed loss of lipid depots and drastically reduced lipid uptake.** *A–F,* using Nile red, epithelium of mutant intestine at P0 (*B*) and P7 (*E*) showed a drastic reduction of lipid droplets as compared with respective controls (*A* and *D*). *C* and *F,* for quantification of the mean fluorescence of lipids per villus. 10–15 villi per animal were taken ($n = 4$, controls; $n = 2$, mutant at postnatal day P0, as well as $n = 4$, controls; and $n = 3$, mutant at postnatal day P6/P7). *G* and *H,* fatty acid uptake by the intestine was markedly reduced in mutant mice (*H*) as compared with controls (*G*). *I,* quantification of the mean fluorescence per villus of NBD-stearic acid uptake 10 min after intestinal administration; 10–15 villi per animal were measured. Shown is one out of three independent experiments with similar results, and $n = 4$ for each group, respectively. *Scale bars,* 100 μm; **, $p < 0.01$. *J* and *K,* electron micrographs stained with ruthenium red. Mutant *Ugcg* f/f/VilCre intestine (*K*) showed loss of microvillar brush border (*mv*) and lack of caveolae (*arrows*) as well as smaller and fewer fat containing lipid droplets (*LD*) in the cytoplasm of enterocytes as compared with wild type control (*J*). *l,* lysosomes; *m,* mitochondria; *scale bars,* 1 μm; *Contr.*, control.

throughout the cytosol of enterocytes in control mice, as shown by anti-GM1 immunofluorescence (Fig. 3*D*). In agreement with TLC GSL analysis, a staining for GM1 was negative in mutant enterocytes (Fig. 3*H*).

Ugcg f/f/VilCre Mice Demonstrated Loss of Fat Deposits—As a consequence of the intestinal GSL deficiency, mutant mice did not gain weight after birth with increasing age (Fig. 4*A, inset*), although they sucked milk normally (Fig. 4*C*). The usual fat deposits in the abdomen and pelvis were not seen in mutants (Fig. 4*E*). Mutant mice regularly defecated attesting a not significantly altered gut motility. However, stools of mutant mice appeared soft and lipid-rich. Offsprings, depleted of intestinal GSLs, succumbed between P5 and P8.

Histology Showed Age-dependent Severe Structural Alterations in Mutant Intestine—In contrast to newborn mutant mice, which showed an inconspicuous morphology at P0, postnatally, between days 5 and 7, the intestinal epithelium demonstrated massively altered structure throughout both the small and large intestines (Fig. 5*A*). The morphology of mucosal villi in all parts of the small intestine was severely distorted in mutants 1 week after birth; they often appeared to be attached or "glued" to one another. In the colon, severe vacuolization was observed in particular in the uppermost layers of the enterocytes.

Cell proliferation in the intestinal epithelium was significantly increased in mutant tissue, with proliferating cells extending to the intestinal lumen. In control litters, proliferating cells were only located in the base of the intestinal crypts (Fig. 5*B, Ki67*). Alkaline phosphatase, usually stringently and continuously located at the apical surface of the intestinal brush border, was detected in a patchy pattern in mutant mice implying a disorganization of microvillar structure (Fig. 5*B*). In comparison with newborn *Ugcg* f/f/VilCre mice at P0, in which the microvillus protein villin was regularly distributed, anti-villin failed to stain the apical brush border region in GSL-deficient enterocytes at P7 (Fig. 5*B*, *villin*).

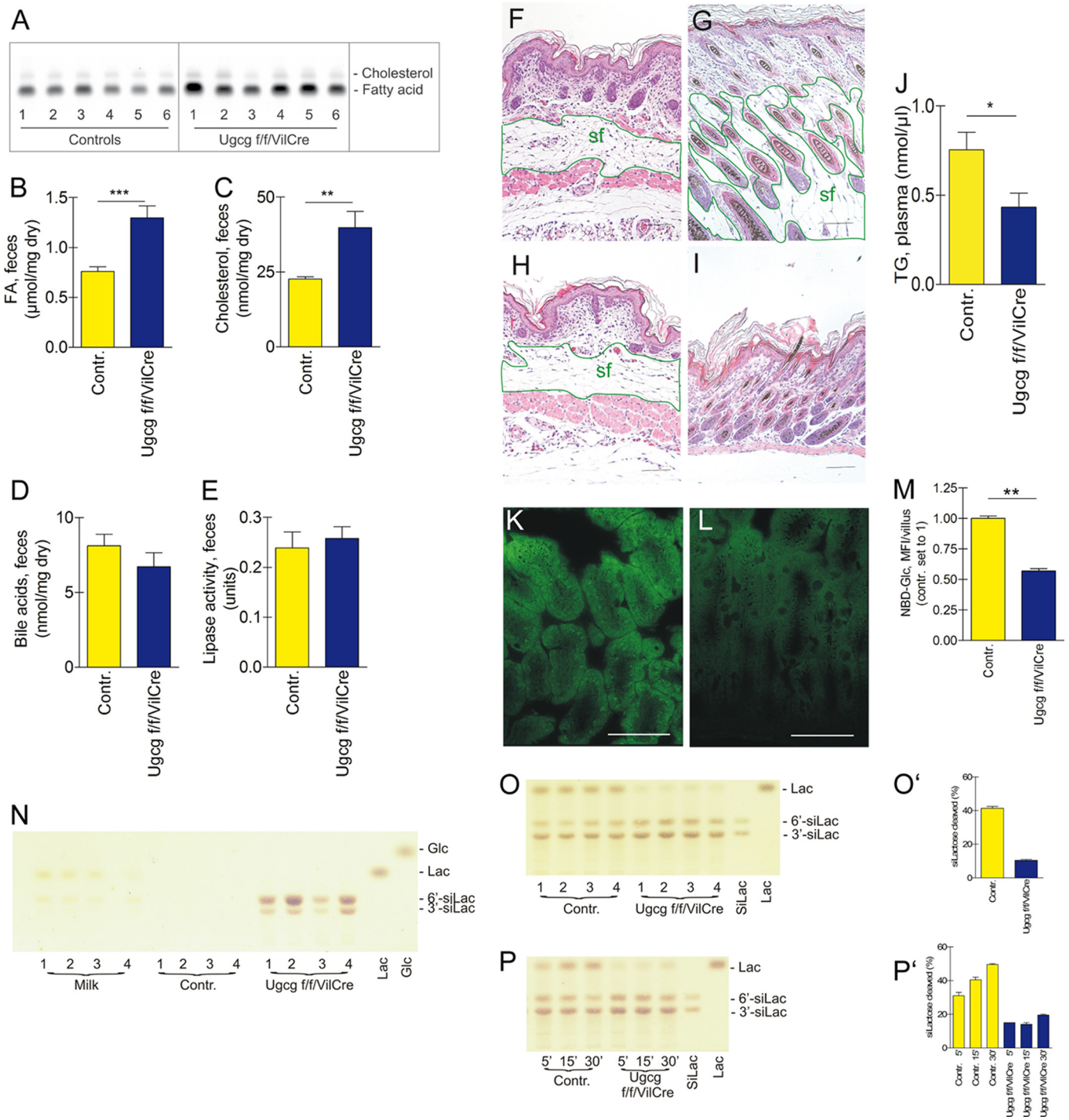

FIGURE 7. ***Ugcg* f/f VilCre mice lost lipids by fecal excretion.** *A–C,* lipids, fatty acids (*A,* TLC; *B,* quantification) ,and cholesterol (*A*, TLC; *C,* quantification) accumulated in feces of *Ugcg*-deficient mice; controls and *Ugcg* f/f/VilCre, $n = 6$ each. *D* and *E,* bile acids (*D*) and lipase activity (*E*) in feces were unaltered indicating their intact secretion from bile duct and pancreas into the intestinal lumen. *F–I, Ugcg* f/f/VilCre mice lost subcutaneous fat deposits. Histology showed that control (*F*) and mutant mice (*H*) had subcutaneous fat tissue (*sf*) on the day of birth, which was no longer present in Ugcg-deficient animals 1 week later (*I*). *G,* in contrast, control animals showed an increased fat storage. *J,* as a consequence of the disturbed intestinal fat uptake, plasma triglyceride concentrations were significantly reduced in mutant mice at P7; controls (*Contr.*), $n = 11$ and *Ugcg* f/f/VilCre, $n = 8$. *K–M, Ugcg* f/f/VilCre mice displayed reduced intestinal glucose uptake. The absorption experiment of NBD-labeled glucose was performed according to uptake of NBD-stearate. Both control (*K*) and mutant newborn mice (*L*) absorbed NBD-glucose. However, the uptake was less in mutant intestine (*L*). *M,* quantification of the medium fluorescence per villus after NBD-glucose uptake, 10 min after intestinal administration; measured were 10–15 villi per animal ($n = 2$, each). *N,* mutant mice were able to absorb lactose after its digestion into galactose and glucose completely but sialylated lactose accumulated in their feces. *O* and *P, Ugcg* f/f VilCre mice showed reduced sialidase activity in the small intestine. Sialidase activity in intestinal cell lysates was measured by digestion of sialylated lactose for 30 min, $n = 4$ for each group (*O*), or in a time-dependent manner as indicated (*P*), and were quantified by a Shimadzu CS 9000 densitometer (*O'* and *P'*); *, $p < 0.05$; **, $p < 0.01$; ***, $p < 0.001$; *scale bars,* 100 μm.

Ugcg f/f/VilCre Mice Displayed Severe Disturbance in Uptake of Nutrients—We thought that absence of GSLs in enterocytes would be associated with a decrease in the uptake of nutrients. Indeed, the lipid marker Nile red indicated a drastic reduction of intracellular lipid depots in *Ugcg* f/f/VilCre mutant mice at P0 (Fig. 6*B*) and P7 (Fig. 6*E*), although controls were strongly stained (Fig. 6, *A* and *D*, and *C* and *F*, quantification). A reduced uptake of NBD-labeled stearic acid further demonstrated the restricted ability of the mutant epithelium to absorb lipids (Fig. 6, *H* and *I*, quantification).

Ultrastructurally, microvilli of enterocytes in control intestines form a regular array of finger-like protrusions (Fig. 6*J*). Different from newborn mice with GSL depletion at P0, postnatally, 1 week after birth, mutant mice displayed only rudimentary stump-like microvilli on the apical surface of enterocytes. The enterocytes of GSL-deficient mice displayed fewer fat containing vacuoles (Fig. 6*K*, *LD*) corroborating the Nile red lipid staining (Fig. 6, *B* and *E*). Caveola-like invaginations as seen in enterocytes of control mice were almost absent in newborn mutants. In addition, their lysosome-like structures appeared smaller than in controls (Fig. 6*K*).

To investigate whether the observed reduced lipid uptake by mutant intestines led to increased fecal lipid excretion, feces of control and mutant mice were investigated for their lipid content. Fatty acids (Fig. 7, *A* and *B*) and cholesterol (Fig. 7, *A* and *C*) significantly accumulated in feces. Secretion of bile acids (Fig. 7*D*) and pancreatic lipases (Fig. 7*E*) into the gut lumen were unaltered indicating that their production and release into the gut lumen were not affected in mutant mice. A subcutaneous fat layer was observed in newborn controls as well as in mutant mice at P0 (Fig. 7, *F* and *H*). Fat deposits were completely used up in mutants until P7 (Fig. 7*I*), whereas controls increased significantly their subcutaneous fat layer (Fig. 7*G*). This showed that the mutant mice metabolized their preterm subcutaneous fat deposits in compensation of the reduced intestinal lipid uptake. In concordance, plasma triglyceride concentrations significantly decreased in mutants (Fig. 7*J*).

To verify whether absorption deficits in mutant intestines were restricted to lipophilic nutrients or also occurred in the uptake of hydrophilic components, the absorption of glucose was investigated. Although Ugcg-deficient mice were able to absorb glucose (Fig. 7*L*), the extent was less than in wild type animals (Fig. 7, *K* and *M*, quantification). The absorption of carbohydrates by the mutant intestine was maintained to an extent that lactose after digestion into galactose and glucose has been completely taken up (Fig. 7*N*). However, sialylated lactose accumulated in feces of *Ugcg* f/f/VilCre mice (Fig. 7*N*) as a consequence of reduced sialidase activity in the small intestine of mutant mice (Fig. 7, *O, O′, P,* and *P′*).

Quantitative RT-PCR was performed to investigate whether altered membrane protein expression negatively influenced the absorption of nutrients in mutant mice. The expression levels of the intestinal fatty acid-binding proteins Fabp2 and CD36, the cholesterol transporters Abcg5 and Abcg8, the triacylglycerol synthesis and transfer proteins Dagt1 and Mttp, the glucose transporters Sglt and Glut5, as well as the small peptide transporter Pept1 were slightly but not significantly altered (Table 5). Our data demonstrate that the functional defects observed were not primarily caused due to alterations of membrane protein expression with one exception, aquaporin 8 (Aqp8). As an indication for reduced water absorption in the small intestine, the mRNA levels of Aqp8 decreased.

TABLE 5
mRNA expression analysis of intestinal proteins

	Relative fluorescence		
Protein	***Ugcg* control**	***Ugcg* f/f/VilCre**	***p***
Fabp2	0.684 ± 0.177	0.543 ± 0.081	0.4612
CD36	0.064 ± 0.029	0.035 ± 0.006	0.2913
Abcg5	1.509 ± 0.208	1.914 ± 0.362	0.3972
Abcg8	1.701 ± 0.336	3.483 ± 0.701	0.0738
Dgat1	0.060 ± 0.023	0.048 ± 0.011	0.6409
Mttp	0.071 ± 0.037	0.142 ± 0.033	0.1818
Sglt	0.085 ± 0.043	0.113 ± 0.028	0.5716
Glut5	0.159 ± 0.034	0.132 ± 0.043	0.6489
Pept1	0.070 ± 0.038	0.035 ± 0.007	0.3117
Aqp8	0.759 ± 0.198	0.010 ± 0.006	0.0035[a]

[a] $p < 0.01$.

Ugcg f/f/VilCreERT2 Mice Similar as Newborn Mutants at P5 to P7 Had Severe Intestinal Alterations Shortly after Induction of the Ugcg Gene Deletion—Besides glucosylceramide, newborn mice synthesize high levels of sialic acid-containing GSLs in the intestine (Figs. 1*F* and 2*A*). In adult mice predominantly glucosylceramide and asialo-GM1 (*GA1,* Fig. 8*A*) can be found (25).

Upon induction with tamoxifen of the specific *Ugcg* gene deletion in the intestine, mice lacked GlcCer and its higher small intestinal synthesis product GA1 almost completely after 4 days (Fig. 8*A*). In heterozygous control mice (*Ugcg* f/+/VilCreERT2), intestinal GSL composition did not change. A reduction of GSL synthesis of 50% was already achieved at day 1 after the start of the tamoxifen induction (Fig. 8*B*). Reduction of 70% of intestinal GSL content accompanied by initial structural alterations was observed 2 days after the start of the tamoxifen application (Fig. 8*B*). An almost complete absence of GSL synthesis and severe structural alterations in the villous epithelia were seen 3 days after beginning tamoxifen treatment (Fig. 8, *B* and *B′*). Our data obtained from the inducible model suggested a critical GSL reduction of ~50–70% to induce relevant structural and functional problems in the intestinal tract. During the time-dependent reduction of GSLs, a drastic decrease in body weight (Fig. 8*C*), food, and water consumption (Fig. 8, *D* and *E*) was observed in mutant mice.

To investigate whether endocytosis of large scale lipid was inhibited by GSL depletion similar to newborn mice, fluorescence-labeled liposomes were injected into the gut lumen of control- and *Ugcg* f/f/VilCreERT2 mice. In this approach we show that liposomes entered the apical membrane of control mice epithelium unimpeded (Fig. 8*F*); in contrast, mutant *Ugcg* f/f/VilCreERT2 mice were not able to absorb liposomes (Fig. 8*F*).

Morphologically, *Ugcg* f/f/VilCreERT2 mice resembled the phenotype of mutant newborns at P5 to P7 (Fig. 9). However, the extent of changes was stronger as in newborns. Adult control- and mutant mice have been injected with EDU on day 2 after the tamoxifen-triggered *Ugcg* gene deletion. One day later, the proliferative zone was seen to be distributed almost throughout the complete epithelial layer, whereas proliferation in tamoxifen-treated controls was restricted to the crypts of the

villi (Fig. 9*B*, *EDU*). Ultrastructurally, similarly as seen in newborn mutant mice 1 week after birth, *Ugcg* f/f/VilCreERT2 mice showed loss of brush border 3–4 days after tamoxifen induction (Fig. 10, *B* and *D*), decreased phospholipid concentrations (Fig. 10*G*), similar sphingomyelin levels as in controls (Fig. 10*H*), and increased ceramide concentrations (Fig. 10*H*).

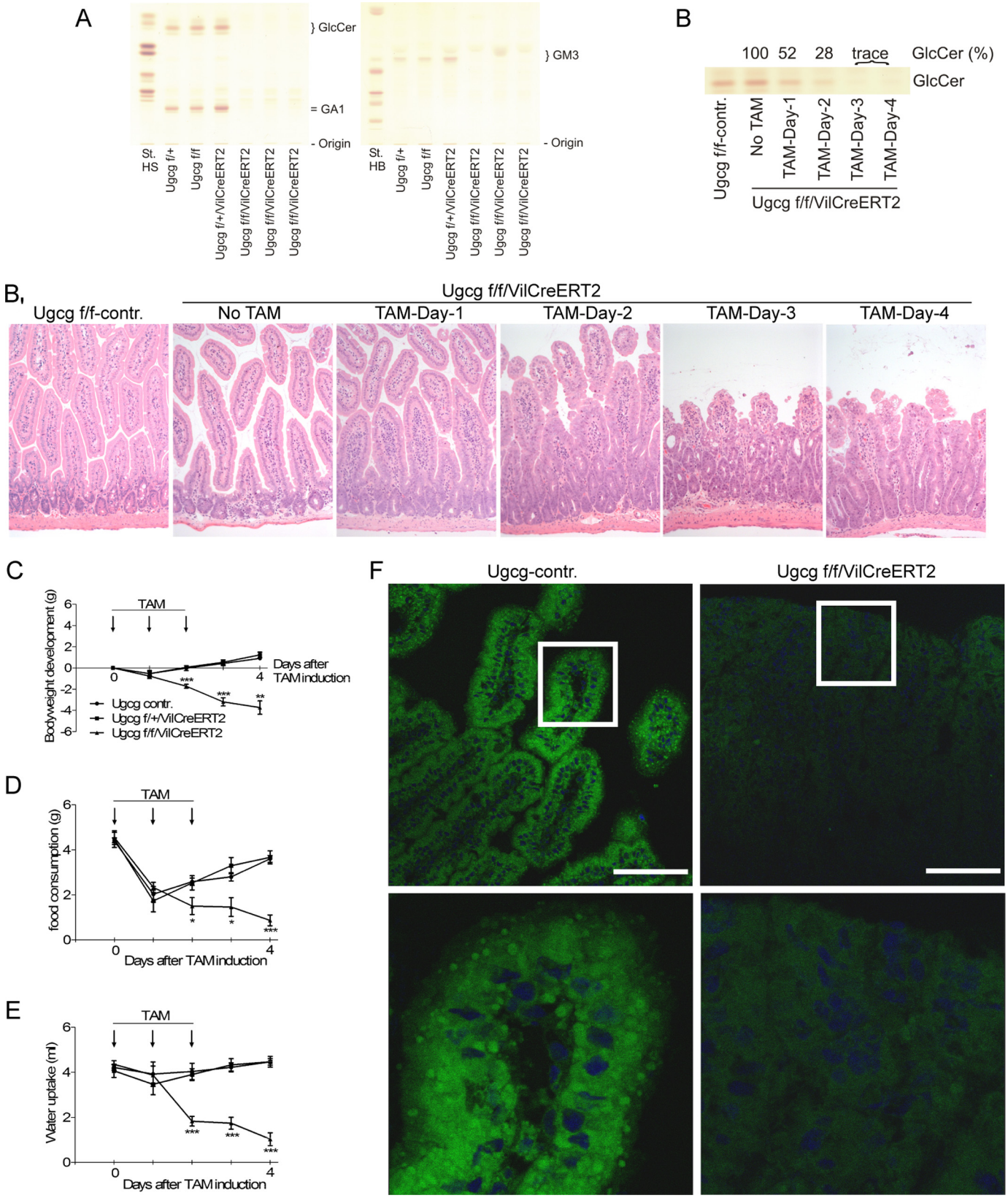

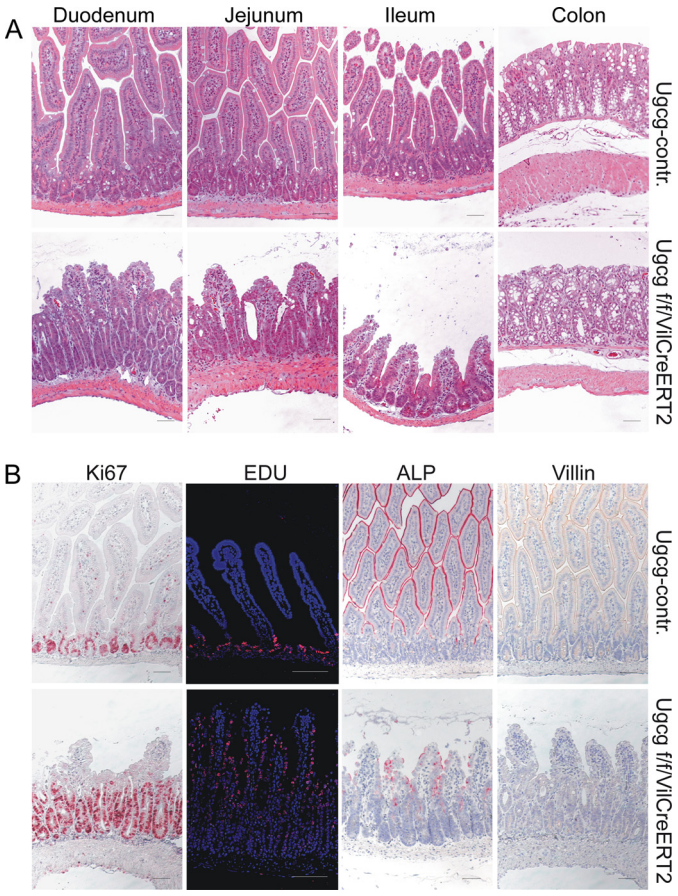

FIGURE 9. **Severe structural defects occurred in small and large intestine of *Ugcg* f/f/VilCreERT2 mice.** *A,* major structural defects similar as in newborn *Ugcg* f/f/VilCre mice 1 week after birth were also recognized in the mucosa of the small and large intestine of *Ugcg* f/f/VilCreERT2 mutant mice 3–4 days upon tamoxifen induction. More obvious than in newborn mutants, in *Ugcg* f/f/VilCreERT2 intestines enterocytes detached from the basal lamina. *B,* highly increased proliferation (Ki67 and EDU) indicated by red nuclei, and drastically decreased expression of the brush border proteins alkaline phosphatase (*ALP*) and villin were observed in tamoxifen-induced mutants devoid of GSL, similar as in newborn *Ugcg* f/f/VilCre mice. *Scale bars,* 100 μm. *Contr.*, control.

Very similar to the GlcCer profile of newborns, GlcCers with a phytosphingosine-containing ceramide anchor were found by LC-MS/MS to be the most prominent species in intestine (Fig. 10*I*). In the intestine of adult mutant mice, GlcCers were drastically reduced (Fig. 10*I*). As in newborns, GlcCers with (d18:1; *n*:0)-ceramide anchors were unaltered. The precursor ceramides increased in mutant tissue significantly (Fig. 10, *H*, *TLC*; and *J*, *LC-MS/MS*). In addition, sphingomyelins (SM) containing phytosphingosine residues were elevated about 5-fold (data not shown). However, these SMs represent only 2% of the total SM content in control intestine. On the other hand, the most prominent SMs in intestine (*i.e.* d18:1;n:0) with sphingosine and nonhydroxylated fatty acid residues decreased roughly by 25% in the mutant tissue. In sum, the total sphingomyelin content in mutant intestine appeared unaltered (Fig. 10, *H*, TLC; and *K*, LC-MS/MS).

Increased ceramide levels may have triggered autophagy (Fig. 10, *B* and *D*) (26, 27), which could be confirmed by elevated Lc3 II expression (Fig. 10, *E* and *F,* quantification). Concomitantly, a significantly higher number of TUNEL-positive cells were seen in tamoxifen-induced *Ugcg* f/f/VilCreERT2 mice (Fig. 10*M*) as compared with newborn *Ugcg* f/f/VilCre animals (Fig. 10*L*).

A detachment of enterocytes from the basal membrane was observed 4 days past tamoxifen induction. To investigate whether this phenomenon occurred due to a dislocation or reduction of adhesion molecules, expression of E-cadherin and β-catenin was investigated. Enterocytes of both control and mutant mice expressed E-cadherin in a basal and basolateral fashion throughout the whole epithelium (Fig. 11*A*). β-Catenin was stained strongly in basal and basolateral regions of control epithelium and in the lower compartments of villi of *Ugcg* f/f/VilCreERT2 mice. However, only partial β-catenin expression or complete absence was seen at the tips of the villi in mutant mice (Fig. 11*B*). Immunofluorescence data could be confirmed by Western blot analysis (Fig. 11, *C* and *D*).

Stromal Immune Cells in Intestine Were Not Changed by the Ugcg Deletion—To investigate whether an infiltration of immune competent mononuclear cells would have triggered the hyperproliferation in mutant intestines, both newborn and adult mutant mice and respective controls were stained for B-cells, T-cells, and monocyte-derived cells. The numbers of immune cells infiltrating intestinal tissue of newborn control mice was very low in general but increased during adulthood (data not shown). However, none of the stainings of mutant newborn and adult intestine showed significant increased numbers of immune cells as compared with the respective control tissues.

Intestinal Phenotype in Ugcg f/f/VilCreERT2 Mice Could Not be Restored by Exogenous GlcCer Feeding—Mutant mice have been fed with chow diet, supplemented with or without 2 mg/g of glucosylceramide *ad libitum*, and both groups were injected with tamoxifen as described. Mutant mice with GlcCer supplementation showed an almost identical decrease in body weight as mutants that received chow diet (data not shown). Animals of both groups had to be sacrificed due to their severely compromised state of health 3 days after the initial tamoxifen induction. Morphologically, GlcCer treated and untreated *Ugcg* f/f/VilCreERT2 mice were undistinguishable (data not shown) suggesting that exogenous GlcCer- application could not compensate for the Ugcg deletion.

Subcellular Localization of Enterocytic GSLs—To verify the role of GSLs for the observed phenotype in mutant mice, their intestinal localization and possible involvement in intracellular

FIGURE 8. ***Ugcg* f/f/VilCreERT2 mice showed severe structural alterations in the intestine shortly after induction of the *Ugcg* gene deletion.** *Ugcg* control and mutant mice were treated for 3 consecutive days with 1 mg of tamoxifen (*TAM*), respectively. *A,* GSLs in the intestine were absent 4 days past the initial tamoxifen application (*left* and *right* TLCs represent neutral and acidic GSLs) and were remarkably reduced by ~50 and ~70% already 1 and 2 days after the initial induction (*B*). The remaining bands in extracts of mutant intestine migrating at the height of GM3 might be explained by admixtures of both intestinal muscle and stroma that were not affected by the *Ugcg* gene deletion. The degree of GSL depletion (*B*) correlated well with the dramatic alterations of the structure of the small intestine as shown by hematoxylin/eosin staining (*B′*). *C–E,* controls and *Ugcg* f/f/VilCreERT2, $n = 5$; heterozygous mice, $n = 3$). Shortly after induction, *Ugcg* f/f/VilCreERT2 mice showed reduction of bodyweight (*C*) as well as a lower food (*D*) and water consumption (*E*). Heterozygous mice developed similar to other controls. *F,* uptake of liposomes is impaired in *Ugcg* f/f/VilCreERT2 mice. Liposomes were rapidly endocytosed by control intestine. In mutant intestine the uptake of liposomes is drastically diminished or absent; *scale bars,* 100 μm. *Contr.*, control.

transport were investigated. In this respect, stainings of GM1 together with the brush border protein villin as well as clathrin and Rab11 were performed in control and mutant mice postnatally at days 5–7.

GM1, ubiquitously distributed in vesicle-like structures in the cytosol of control mice postnatally at day P0 (see Fig. 3*D*), concentrated apically below the brush border 1 week after birth (Fig. 12, *A*, *C*, and *E*). Only a small overlap could be seen

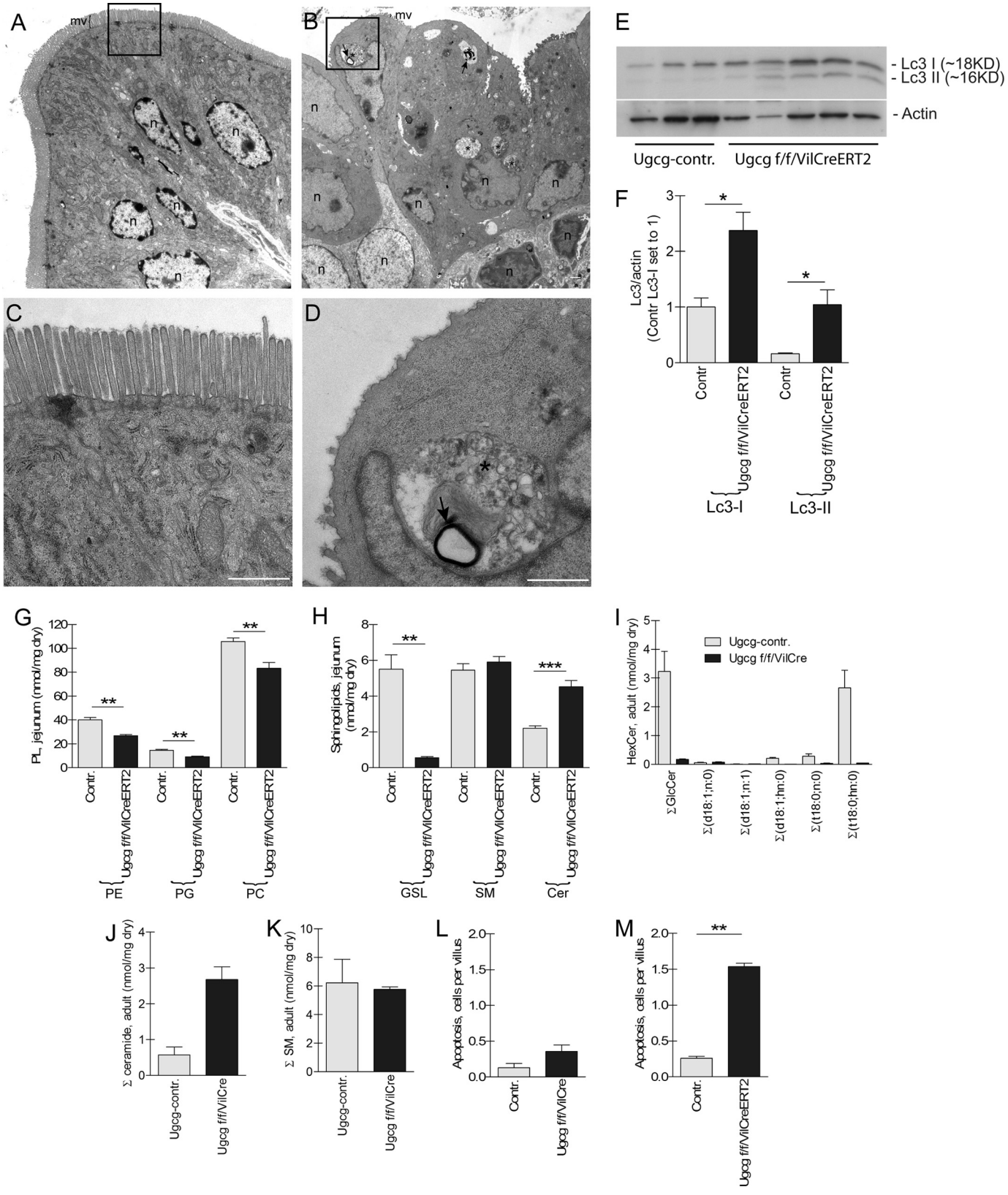

between GM1 and villin in the microvillar region of the wild type intestine (Fig. 12*A*). GM1 stained negative in mutant tissue, and the brush border protein villin was detected only rudimentarily. A costaining of GM1 with clathrin, one marker of coated pits and vesicles (Fig. 12*C*) as well as GM1 with the recycling endosomal marker protein Rab11 (Fig. 12*E*) in control tissue, indicated close proximity apically below the brush border. GM1 similarly as at P0 was again not stained in mutant tissue (Fig. 12, *D* and *F*). The expression of clathrin and Rab11 was drastically down-regulated in mutant tissue 1 week after birth (Fig. 12, *D* and *F*). In addition, also the lysosomal marker Lamp1 decreased in *Ugcg* f/f/VilCre intestine (Fig. 12*H*).

The data obtained by immunofluorescence could be confirmed with Western blot analysis. The expression of proteins involved in endocytotic processes and in protein recycling such as clathrin, caveolin-1, and Rab11 was drastically down-regulated (Fig. 12, *G* and *J*). However, the early endosomal marker proteins Rab4 and Rab5 were not significantly altered (Fig. 12*K*).

GSLs Cluster in Vesicles and Are Located Predominantly Below or Close to the Brush Border—Confocal immunofluorescence images have a limited resolution. To answer the question whether GSLs were involved in membrane events such as formation of caveolae and transport vesicles, immunogold EM stainings have been performed to elucidate the exact intracellular localization of GM1 in newborn (P5) as well as GA1 in adult mice. GM1 was found to be predominantly located in vesicle-like structures (Fig. 13*A, arrows*). These vesicles showed two opposite migration directions. The vesicular content, including GSLs, was shed into the intestinal lumen where GSLs have been found in the glycocalyx (Fig. 13, *A* and *B*) and also was released into lipid droplets (Fig. 13*C*). Absence of GM1 went along with an almost complete absence of lipid droplets in *Ugcg* f/f/VilCre mice (Fig. 13*D*).

A costaining of GM1 with clathrin demonstrated that coated pits formed at the apical membrane surface (Fig. 13*E*) mostly independent from GSLs; only a few gold particles that labeled clathrin were associated with GSL vesicles (Fig. 13*E*). Specific staining for GM1 and clathrin did not occur in mutant tissue. In GM1 and Rab11 coimmune EM, Rab11 was (with a few exceptions (Fig. 13*G, inset*)) not directly associated with GSL vesicles (Fig. 13*G*). Our immune electron microscopic data suggested that GSL vesicle formation essentially did not depend on clathrin and Rab11.

Similar to newborn mice, in adult animals GSL (GA1) could be visualized in vesicle-like structures (Fig. 13*I, arrows*). Those vesicles appeared to be released into the intestinal lumen (Fig. 13*J*) and again attached to lipid depots (Fig. 13*K*). *Ugcg* f/f/VilCreERT2 tissue showed only few dots of background staining (Fig. 13*L*).

DISCUSSION

This study reports new insights into the role of GSLs for intestinal epithelial function. GSLs have been surmised to be important for epithelial polarization (28) and differentiation (29). Indeed, in *C. elegans* mutants in whom GSL synthesis was inhibited by feeding of RNAi against glucosylceramide synthase (Ugcg), an impaired distribution of proteins involved in intestinal polarization such as ERM-1 and actin has been shown. A depletion rate of ~75% of glucosylceramide was sufficient to induce those dramatic defects (11).

Are these results also to be expected in mammals? Based on our data with GSL depletion in the liver in which bile canalicular function was maintained (16), we have postulated a different function of GSLs in mouse enterocytes but for epithelial polarity. Two mouse models, an inducible model in adult mice and a constitutive model in which GSLs were depleted during embryogenesis, were applied. The latter model provided the advantage to investigate the morphology of the intestine shortly after birth when its absorptive activity was not yet fully developed. Such a state of functional quiescence cannot be tested in *C. elegans,* and might be one reason that a similar phenotype has not been observed in worms. Surprisingly, the intestine of newborn mutants at P0 could neither macroscopically nor by microscopy be distinguished from that of control littermates, but the mutants lacked GSLs in the intestine. Also, epithelial proliferation did not differ from control intestine at P0, suggesting that GSL depletion had no immediate influence on the cell cycle of enterocytes. An epithelial-to-mesenchymal transition process in which GSLs were described to play a critical role *in vitro* (30, 31) also did not occur as enterocyte morphology appeared normal at that stage and enterocytes seemed fully differentiated and polarized. However, newborn mutant offspring at P0 were not able to absorb milk fat in a similar amount as their control littermates. This was an initial hint that GSLs might be directly involved in lipid absorption and/or transport. The finding that villin, a marker of enterocytic polarization, was unchanged in GSL-depleted intestine at P0 and that the brush border was regularly formed suggested that GSLs were not immediately needed for microvillar generation and consequently for epithelial enterocytic polarization. This observation

FIGURE 10. **Tamoxifen-induced *Ugcg* f/f/VilCreERT2 mice show loss of brush border as well as increased autophagy and apoptosis.** *A–D,* electron micrographs of adult control mice (*A* and *C,* magnification) and tamoxifen-induced *Ugcg* f/f/VilCreERT2 mice (*B* and *D*, magnification). Sections were stained according to Karnovsky *et al.* (19). Adult mice lacking GSLs in enterocytes showed loss of brush border (*B* and *D*) similar as seen in newborn mutants. In addition, increased numbers of multivesicular bodies (*) and marked autophagy (*arrows*) were detected in the cytoplasm of enterocytes of induced mutant mice (*B* and *D*); *scale bars,* 1 μm. *E,* Lc3 II expression, a marker of autophagy, was significantly elevated in tamoxifen-induced *Ugcg* f/f/VilCreERT2 mice as compared with their respective controls (*F,* quantification). *G,* similar as in *Ugcg* f/f/VilCre newborn mutant mice 1 week after birth; the phospholipid concentration in the intestine decreased significantly; controls, $n = 6$, and *Ugcg* f/f/VilCre, $n = 4$. *H,* as revealed by TLC analysis, ceramide concentration in jejunum of *Ugcg* f/f/VilCreERT2 increased significantly and was stronger than in newborn mutant mice. The total sphingomyelin (*SM*) content was not altered; controls, $n = 6$, and *Ugcg* f/f/VilCre, $n = 4$. *I–K,* LC-MS/MS quantification of GlcCers, ceramides, and SM. *I,* total GlcCer depletion rate in adult *Ugcg* f/f/VilCreERT2 mutants reached similar levels (>90%) as in newborn mice at P0 (controls and mutant, $n = 3$, respectively). Similar as in newborns, a GlcCer fraction with sphingosine and nonhydroxylated fatty acids in its ceramide anchor was not affected by the *Ugcg* gene deletion. *J,* further MS analysis indicated that ceramide levels increased in mutant tissue and confirmed the data obtained from TLC analysis. *K,* total SM levels were similar in control and mutant intestine; however, the SM composition changed qualitatively (data not shown). *L* and *M,* increased ceramide concentrations in enterocytes may have contributed to the higher number of TUNEL-positive cells per villus in tamoxifen-induced adult mutant *Ugcg* f/f/VilCreERT2 (*M*) as compared with newborn *Ugcg* f/f/VilCre mice (*L*); $n = 4$ each. *, $p < 0.05$; **, $p < 0.01$; ***, $p < 0.001$. *Contr.*, control.

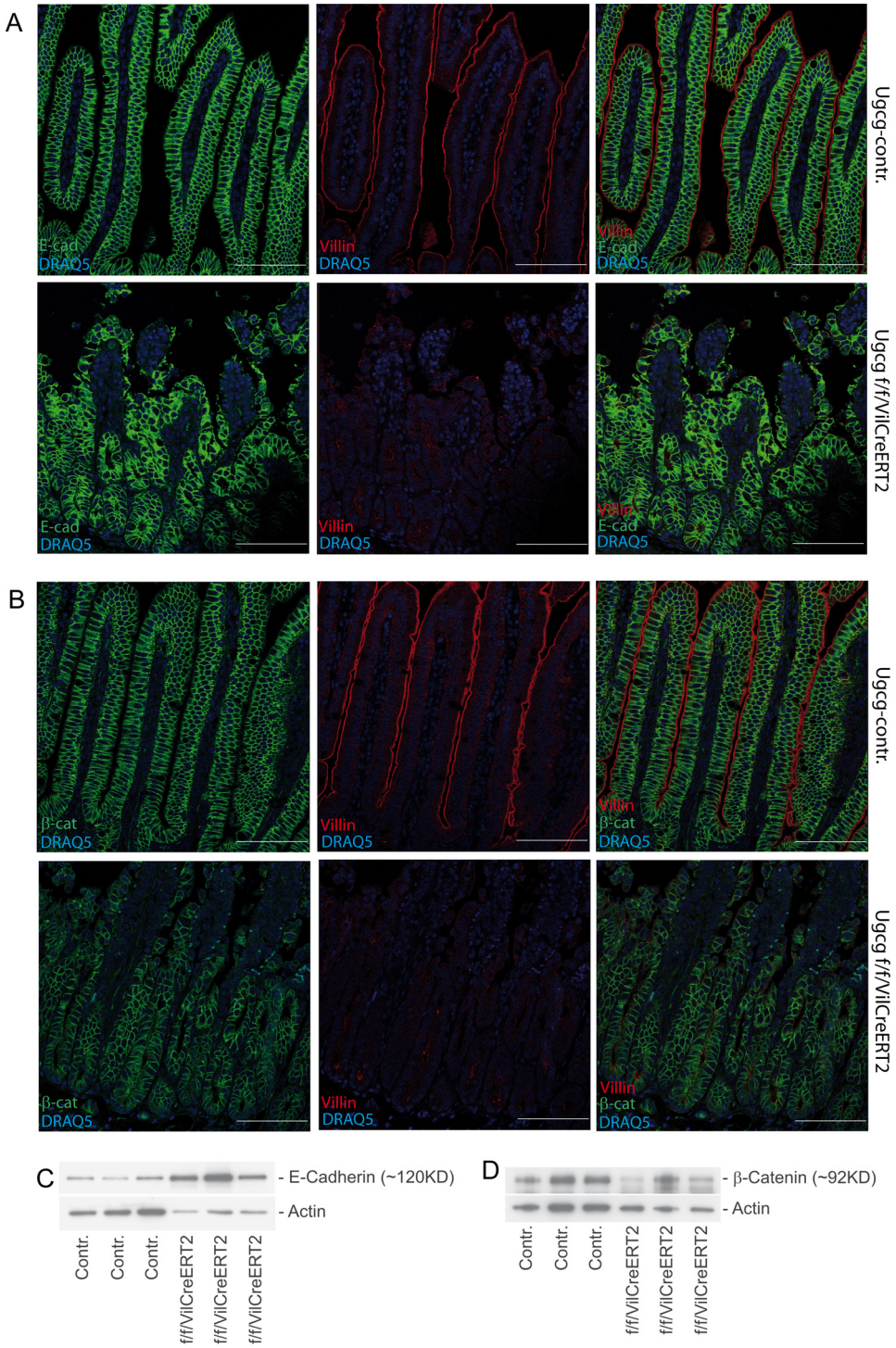

FIGURE 11. ***Ugcg* f/f/VilCreERT2 mice showed reduced expression of β-catenin in luminal epithelial cells at day 4 upon tamoxifen treatment.** *A* and *B,* villous epithelial cells were stained with an anti E-cadherin- (*A*) or β-catenin antibody (*B*). The apical brush border was counterstained with anti-villin. E-cadherin accumulated in enterocytes (*A*). Particularly in the heads of villi of mutant mice, detachment of enterocytes from the basal membrane and consequently partial disruption of the columnar epithelium occurred, and also β-catenin staining was reduced in *Ugcg* f/f/VilCreERT2 mice (*B*); *scale bars,* 100 μm. *C* and *D,* results obtained by immunofluorescence could be confirmed by Western blot analysis. *Contr.*, control.

corroborated the results from mouse models with GSL depletion in liver (16) and in kidney.[4] In these organs, neither hepatocytic autoplasmic microvillus-like protrusions into canaliculi of hepatocytic epithelial cells nor microvilli of the proximal renal epithelium were altered upon GSL depletion. The latter findings implied the question of the cellular localization of GSLs in enterocytes. We surmised that GSL could be associated with proteins involved in intracellular transport. In control mice a few days after birth, we could demonstrate, by confocal microscopy and more clearly by immune electron microscopy,

[4] P. Stettner, H.-J. Gröne, and R. Jennemann, unpublished data.

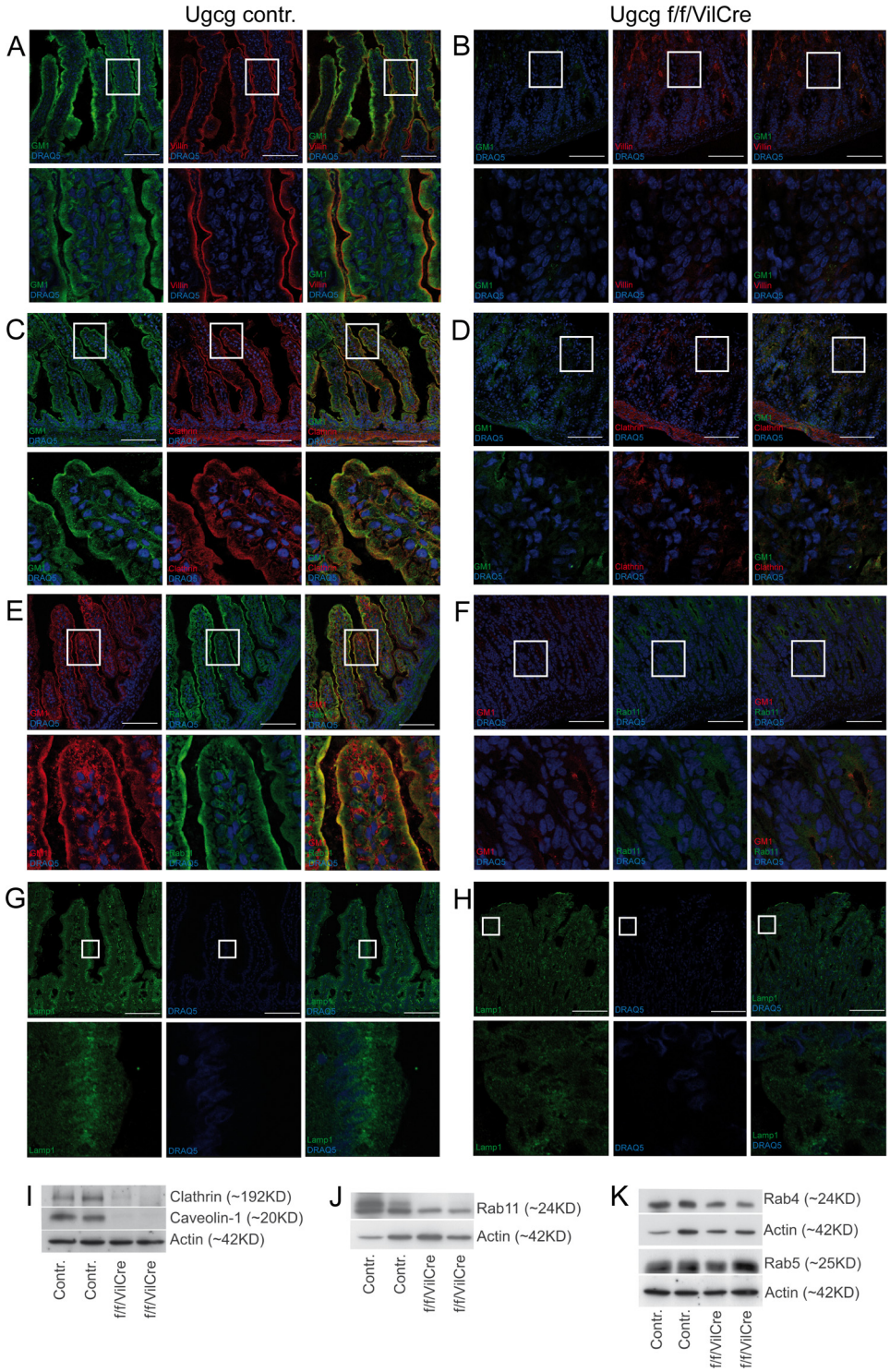

FIGURE 12. **GM1 to a major extent was found apically in vesicular structures in the cytosol and stained negative in mutant mouse tissue.** All stainings shown were performed on intestinal jejunum sections collected 5–7 days after birth. Animals of the same age (littermates) were compared. *A* and *B,* costaining of GM1 together with villin. In contrast to newborn mice at day P0 in which GM1 was ubiquitously located in small dots in the cytosol of the epithelium, 1 week after birth GM1 located predominantly on the apical site of the enterocytes (*A*). The structural protein villin was stained in the brush border, but only a small overlap could be seen together with GM1. GM1 was stained to a major extent apically, apart from the brush border. *B,* in mutant tissue, as expected, GM1 could not be detected but also villin expression was very weak. *C* and *D,* costaining of GM1 and clathrin. In control tissue GM1 and clathrin were found in similar regions apically in the enterocytes (*C*). Clathrin expression was much less pronounced in mutant epithelium but was still present in the intestinal zona muscularis propria (*D*). *E* and *F,* costaining of GM1 together with the recycling endosomal marker protein Rab11. GM1 could be located apically in similar regions as Rab11 (*E*). Rab11 staining in mutant intestine was very weak (*F*). *G,* Lamp1-positive lysosomes were stained and were regularly distributed in the cytosol of the intestinal epithelium of control mice. *H,* in mutant tissue, Lamp1 staining appeared weaker, and lysosomes were irregularly distributed within the cytosol of the enterocytes. *I–K,* Western blot analysis revealed drastically decreased levels of clathrin and caveolin-1, proteins involved in endocytosis (*I*) as well as Rab11 as a marker for recycling endosomes important for protein recycling (*J*). The early endosomal marker proteins Rab4 and Rab5 showed similar expression in control and mutant tissue (*K*). *Contr.*, control.

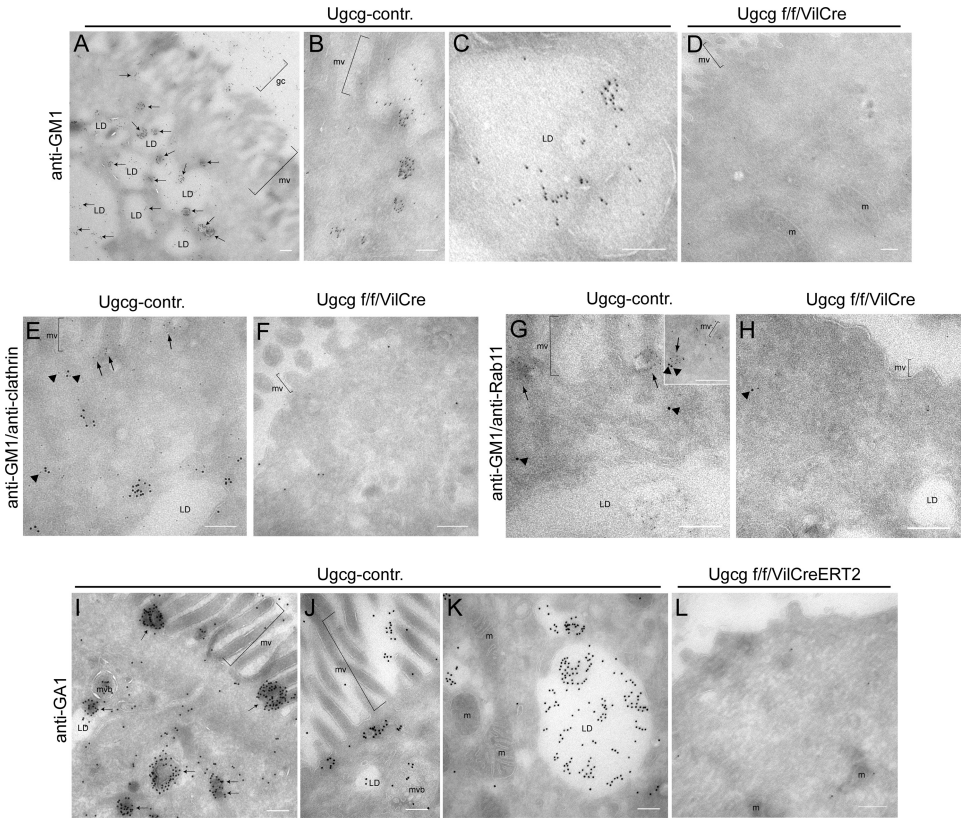

FIGURE 13. **By immune electron microscopy, GSLs predominantly localize in vesicles close to the brush border.** *A–C,* immunogold EM stainings of GM1 in control intestine of newborn mice at P5. GM1 was visualized associated in vesicles, below the brush border (*mv*) and in the region of the glycocalyx (*gc*) (*A, arrows*). Only rudimentary staining was seen in the microvilli. *B,* GSL-containing vesicles seemed to release their content at the apical membrane of the enterocytes into the intestinal lumen and intracellularly into lipid depots (*LD*) (*A* and *C*). *D,* only scarce unspecific gold particles were observed in enterocytes of *Ugcg* f/f/VilCre mice. *E* and *F,* immunogold EM costaining of GM1 (10 nm gold particles) with clathrin (5-nm gold particles) in newborn control (*E*) and mutant mice (*F*) at P5. Clathrin-coated pits (*arrows*) originate in wild type mice mostly independent from GSLs at the apical membrane of the enterocytes (*E*). Only few clathrin-positive dots colocalized with GM1 vesicles (*arrowheads*). In mutant mice GM1 and clathrin were almost completely absent (*F*). *G,* similar as clathrin, also Rab11 (10-nm gold particles, *arrowheads*) predominantly did not colocalize with GM1 vesicles (*G, arrows,* 5-nm gold particles) with a few exceptions (*inset*). *H,* only a background staining for GM1 and a reduced Rab11 staining was seen in mutant tissue. *I–L,* in adult animals, the GSL GA1, similar as GM1 in newborns, also localized in vesicles. GSL (*GA1*)-associated vesicles (*I, arrows*) are present in a layer close to the brush border (*J*) or in lipid droplets (*LD*) (*K*) similarly to the location of GSLs in newborn animals 1 week after birth. *L, Ugcg* f/f/VilCreERT2 intestine showed only a few unspecific gold particles; *m*, mitochondria; *scale bars,* 200 nm. *Contr.*, control.

the existence of small GSL-containing vesicles at the apical membrane located below the brush border in the cytosol, similar to data reported earlier (3). These vesicles followed a transport route from the apical membrane to the enterocytic lipid depots and hence seemed to be involved in endocytosis and intracellular transport of nutritional lipids. The GSL-dependent vesicle formation, essentially devoid of clathrin and Rab11, which are also involved in endocytosis and recycling processes (32–35), might be unique for the intestine due to its high concentration of glycosphingolipids. The question whether GSL vesicles require proteins for their formation still remains to be elucidated. Because of the disturbed lipid absorption, the intestine reacted with hyperproliferation; infiltration of immune cells that potentially may have triggered such a process could not be observed. As consequence of the epithelial hyperproliferation, a regular differentiation of the enterocytes was inhibited. Usually, in wild type animals, the intestinal epithelium exhibits a small proliferative area located in the crypts of villi. Cells differentiate into enterocytes and, while migrating to the apex of the villus, exert their absorptive function; they are then released into the gut lumen after 3–5 days (36). In our mutant mice, with fully developed phenotype, the proliferative zone was not restricted to the crypts of the villi, and it extended to half of the epithelium or even higher if associated with immature differentiation of the epithelial enterocytes 5–7 days after birth or 3–4 days after tamoxifen-induced *Ugcg* deletion in adult animals. The altered epithelial differentiation could also be depicted by the rudimentary formation of the brush border. It should be stressed, however, that GSL depletion did not primarily induce hyperproliferation, because in newborn mice with GSL deficiency, the proliferative rate of enterocytes was comparable with control mice.

Caveolin-dependent invaginations have been proposed to be involved in several biological processes such as cell signaling, membrane traffic (2, 37), and endocytosis (3). It cannot be definitively decided whether a disturbed epithelial differentiation might have been accompanied with a reduced expression of caveolin or its intracellular recycling was affected. In our GSL-deficient mice, a significant reduction of caveolae formation was indicated by electron microscopy and Western blot.

Although the structural alterations in the intestine after Ugcg deletion appeared very prominent, the mRNA expression levels of proteins, actively thought to be involved in lipid binding and intracellular transport, were essentially unaltered. Nei-

ther the intestinal fatty acid-binding proteins Fabp2 and CD36 nor enzymes important for triglyceride synthesis and transfer such as Dgat1 and Mttp were statistically significantly changed. Also the intestinal cholesterol transporters Abcg5 and Abcg8 as well as the short chain peptide transporter Pept1 and the glucose transporters Sglt1 and Glu5 were not significantly altered. However, the down-regulation of the membrane integral protein Aqp8, which has been described to function on the apical side of duodenum, jejunum, and colon (38), was accompanied by a lower intestinal water absorption associated with a significant increase of hematocrit levels in *Ugcg* f/f/VilCreERT2 mice (data not shown). Reduced expression and activity of Aqp8 water channels may have been one factor for the extreme soft stools observed in mutant mice.

Fat from nutrients, predominantly in the form of triglycerides, is primarily cleaved into monoacylglycerols and free fatty acids by secreted pancreatic lipases. The first step in lipid absorption, the movement of monoacylglycerols and fatty acids across the apical membrane of enterocytes, is not well defined on a molecular level; it very likely involves different mechanisms. Several studies describe protein-dependent mechanisms, although others have reported protein-independent transport via diffusion through the apical membrane of the enterocytes (39, 40) for which in particular bile salts appear to be necessary as they form micelles with the fatty acids and facilitate thereby their absorption (41). Lipids also might be taken up via endocytosis. *Ex vivo*, in intestinal tissue sections it could also be shown that exposure of high lipid concentrations led to increased formation of clathrin-containing invaginations and vesicles that were then transported and released to intracellular lipid depots (42). This lipid uptake process appears to be particularly important when the lipid concentration in the intestine is extremely high such as in the situation of newborn suckling mice receiving high fat milk. Indeed, in our *in vivo* studies, we now could demonstrate that large scale fat from milk and in the form of liposomes can be endocytosed. However, this process depended on GSL expression. In support, caveolar endocytosis in ovary cells was significantly reduced after GSL depletion by inhibition of GSL synthesis (43).

Intestinal GlcCers predominantly express phytosphingosine with α-hydroxylated fatty acid in their ceramide anchor. In particular, in the adult intestinal model, most of this GlcCer accumulated in the form of its precursor ceramide, and only about 1/5 of it was shuttled into phytosphingosine-containing SM. This is in contrast to what we had found previously in brain and liver, where almost all of the ceramide that could not be converted to GlcCer was shifted into sphingomyelin (12, 16). However, to a similar extent as phospholipids, the major sphingosine-containing SM fraction decreased, probably as a consequence of loss of the brush border accompanied with loss of membrane. Increased ceramide accumulations particularly occurring in adult *Ugcg*-deficient mutants may have triggered the pronounced autophagy (26, 27) and apoptosis.

β- and α-catenin form complexes with E-cadherin that are important for anchoring epithelial cells to the lamina propria. In adult tamoxifen-induced mutant mice, a lowered expression of β-catenin has been observed, which may have facilitated the detachment of enterocytes. Moreover, it has been demonstrated that β-catenin binds GA1, which is the prominent GSL in adult enterocytes. GSL depletion may have indirectly also negatively influenced the epithelial binding to the basal lamina (31).

The phenotype observed in our mutant mice could not be alleviated by the uptake of exogenous GSL via milk or by adding GlcCer to the food. In this respect, it has been convincingly shown that exogenously applied GSL was almost completely degraded (44–47).

GSL expression in the intestine very likely may not have been influenced by an uptake of shed liver GSL via the blood as their concentration in the blood is very low. In addition, the blood GSL pattern differs from the intestinal GSL, and in particular the main GlcCer bands in the neutral GSLs showed a different migration speed as GlcCers from blood and milk (data not shown), suggesting a different ceramide anchor as the ones mainly found in intestinal GSLs.

In summary, glycosphingolipid expression in the intestinal epithelium is quintessential for maintenance of a GSL signature of absorption-dependent intracellular transport and intestinal structure. However, GSLs are not primarily required for enterocyte-polarized brush border formation.

Acknowledgments—The technical support of Gabi Schmidt and Claudia Schmidt is gratefully acknowledged. We are grateful to John F. Bertram (Department of Anatomy and Developmental Biology, Monash University, Melbourne, Australia) and Bernd Arnold (Molecular Immunology, DKFZ, Germany) for critical input to the manuscript.

REFERENCES

1. Christiansen, K., and Carlsen, J. (1981) Microvillus membrane vesicles from pig small intestine. Purity and lipid composition. *Biochim. Biophys. Acta* **647,** 188–195
2. Lingwood, D., and Simons, K. (2010) Lipid rafts as a membrane-organizing principle. *Science* **327,** 46–50
3. Hansen, G. H., Pedersen, J., Niels-Christiansen, L. L., Immerdal, L., and Danielsen, E. M. (2003) Deep-apical tubules. Dynamic lipid-raft microdomains in the brush-border region of enterocytes. *Biochem. J.* **373,** 125–132
4. Tamboli, I. Y., Prager, K., Barth, E., Heneka, M., Sandhoff, K., and Walter, J. (2005) Inhibition of glycosphingolipid biosynthesis reduces secretion of the β-amyloid precursor protein and amyloid β-peptide. *J. Biol. Chem.* **280,** 28110–28117
5. Sprong, H., Degroote, S., Claessens, T., van Drunen, J., Oorschot, V., Westerink, B. H., Hirabayashi, Y., Klumperman, J., van der Sluijs, P., and van Meer, G. (2001) Glycosphingolipids are required for sorting melanosomal proteins in the Golgi complex. *J. Cell Biol.* **155,** 369–380
6. Yamashita, T., Hashiramoto, A., Haluzik, M., Mizukami, H., Beck, S., Norton, A., Kono, M., Tsuji, S., Daniotti, J. L., Werth, N., Sandhoff, R., Sandhoff, K., and Proia, R. L. (2003) Enhanced insulin sensitivity in mice lacking ganglioside GM3. *Proc. Natl. Acad. Sci. U.S.A.* **100,** 3445–3449
7. Kabayama, K., Sato, T., Saito, K., Loberto, N., Prinetti, A., Sonnino, S., Kinjo, M., Igarashi, Y., and Inokuchi, J. (2007) Dissociation of the insulin receptor and caveolin-1 complex by ganglioside GM3 in the state of insulin resistance. *Proc. Natl. Acad. Sci. U.S.A.* **104,** 13678–13683
8. Liu, Y., Su, Y., Wiznitzer, M., Epifano, O., and Ladisch, S. (2008) Ganglioside depletion and EGF responses of human GM3 synthase-deficient fibroblasts. *Glycobiology* **18,** 593–601
9. Yoon, S. J., Nakayama, K., Hikita, T., Handa, K., and Hakomori, S. I. (2006) Epidermal growth factor receptor tyrosine kinase is modulated by GM3 interaction with *N*-linked GlcNAc termini of the receptor. *Proc. Natl. Acad. Sci. U.S.A.* **103,** 18987–18991

10. Marza, E., Simonsen, K. T., Faergeman, N. J., and Lesa, G. M. (2009) Expression of ceramide glucosyltransferases, which are essential for glycosphingolipid synthesis, is only required in a small subset of *C. elegans* cells. *J. Cell Sci.* **122,** 822–833
11. Zhang, H., Abraham, N., Khan, L. A., Hall, D. H., Fleming, J. T., and Göbel, V. (2011) Apicobasal domain identities of expanding tubular membranes depend on glycosphingolipid biosynthesis. *Nat Cell Biol.* **13,** 1189–1201
12. Jennemann, R., Sandhoff, R., Wang, S., Kiss, E., Gretz, N., Zuliani, C., Martin-Villalba, A., Jäger, R., Schorle, H., Kenzelmann, M., Bonrouhi, M., Wiegandt, H., and Gröne, H. J. (2005) Cell-specific deletion of glucosylceramide synthase in brain leads to severe neural defects after birth. *Proc. Natl. Acad. Sci. U.S.A.* **102,** 12459–12464
13. Madison, B. B., Dunbar, L., Qiao, X. T., Braunstein, K., Braunstein, E., and Gumucio, D. L. (2002) Cis elements of the villin gene control expression in restricted domains of the vertical (crypt) and horizontal (duodenum, cecum) axes of the intestine. *J. Biol. Chem.* **277,** 33275–33283
14. Maunoury, R., Robine, S., Pringault, E., Léonard, N., Gaillard, J. A., and Louvard, D. (1992) Developmental regulation of villin gene expression in the epithelial cell lineages of mouse digestive and urogenital tracts. *Development* **115,** 717–728
15. el Marjou, F., Janssen, K. P., Chang, B. H., Li, M., Hindie, V., Chan, L., Louvard, D., Chambon, P., Metzger, D., and Robine, S. (2004) Tissue-specific and inducible Cre-mediated recombination in the gut epithelium. *Genesis* **39,** 186–193
16. Jennemann, R., Rothermel, U., Wang, S., Sandhoff, R., Kaden, S., Out, R., van Berkel, T. J., Aerts, J. M., Ghauharali, K., Sticht, C., and Gröne, H. J. (2010) Hepatic glycosphingolipid deficiency and liver function in mice. *Hepatology* **51,** 1799–1809
17. Dickson, J. J., and Messer, M. (1978) Intestinal neuraminidase activity of suckling rats and other mammals. Relationship to the sialic acid content of milk. *Biochem. J.* **170,** 407–413
18. Salic, A., and Mitchison, T. J. (2008) A chemical method for fast and sensitive detection of DNA synthesis *in vivo*. *Proc. Natl. Acad. Sci. U.S.A.* **105,** 2415–2420
19. Karnovsky, M. J. (1967) The ultrastructural basis of capillary permeability studied with peroxidase as a tracer. *J. Cell Biol.* **35,** 213–236
20. Tokuyasu, K. T. (1997) in *Cells: A Laboratory Manual* (Spector, D. L., Goodman, R. D., and Leinwand, L. A., eds) Cold Spring Harbor Laboratory Press, Cold Spring Harbor, NY
21. Jennemann, R., Rabionet, M., Gorgas, K., Epstein, S., Dalpke, A., Rothermel, U., Bayerle, A., van der Hoeven, F., Imgrund, S., Kirsch, J., Nickel, W., Willecke, K., Riezman, H., Gröne, H. J., and Sandhoff, R. (2012) Loss of ceramide synthase 3 causes lethal skin barrier disruption. *Hum. Mol. Genet.* **21,** 586–608
22. Chomczynski, P., and Sacchi, N. (1987) Single-step method of RNA isolation by acid guanidinium thiocyanate/phenol/chloroform extraction. *Anal. Biochem.* **162,** 156–159
23. Ma, T., Jayaraman, S., Wang, K. S., Song, Y., Yang, B., Li, J., Bastidas, J. A., and Verkman, A. S. (2001) Defective dietary fat processing in transgenic mice lacking aquaporin-1 water channels. *Am. J. Physiol. Cell Physiol.* **280,** C126–C134
24. IUPAC-IUB Joint Commission on Biochemical Nomenclature (1999) IUPAC-IUB Joint Commission on Biochemical Nomenclature (JCBN) of Glycolipids Recommendations 1997 *J. Mol. Biol.* **286,** 963–970
25. Yoneshige, A., Sasaki, A., Miyazaki, M., Kojima, N., Suzuki, A., and Matsuda, J. (2010) Developmental changes in glycolipids and synchronized expression of nutrient transporters in the mouse small intestine. *J. Nutr. Biochem.* **21,** 214–226
26. Daido, S., Kanzawa, T., Yamamoto, A., Takeuchi, H., Kondo, Y., and Kondo, S. (2004) Pivotal role of the cell death factor BNIP3 in ceramide-induced autophagic cell death in malignant glioma cells. *Cancer Res.* **64,** 4286–4293
27. Hou, Q., Jin, J., Zhou, H., Novgorodov, S. A., Bielawska, A., Szulc, Z. M., Hannun, Y. A., Obeid, L. M., and Hsu, Y. T. (2011) Mitochondrially targeted ceramides preferentially promote autophagy, retard cell growth, and induce apoptosis. *J. Lipid Res.* **52,** 278–288
28. Hoekstra, D., Maier, O., van der Wouden, J. M., Slimane, T. A., and van IJzendoorn, S. C. (2003) Membrane dynamics and cell polarity. The role of sphingolipids. *J. Lipid Res.* **44,** 869–877
29. Pescio, L. G., Favale, N. O., Márquez, M. G., and Sterin-Speziale, N. B. (2012) Glycosphingolipid synthesis is essential for MDCK cell differentiation. *Biochim. Biophys. Acta* **1821,** 884–994
30. Guan, F., Handa, K., and Hakomori, S. I. (2009) Specific glycosphingolipids mediate epithelial-to-mesenchymal transition of human and mouse epithelial cell lines. *Proc. Natl. Acad. Sci. U.S.A.* **106,** 7461–7466
31. Guan, F., Schaffer, L., Handa, K., and Hakomori, S. I. (2010) Functional role of gangliotetraosylceramide in epithelial-to-mesenchymal transition process induced by hypoxia and by TGF-β. *FASEB J.* **24,** 4889–4903
32. McMahon, H. T., and Boucrot, E. (2011) Molecular mechanism and physiological functions of clathrin-mediated endocytosis. *Nat. Rev. Mol. Cell Biol.* **12,** 517–533
33. Boettner, D. R., Chi, R. J., and Lemmon, S. K. (2012) Lessons from yeast for clathrin-mediated endocytosis. *Nat. Cell Biol.* **14,** 2–10
34. Anitei, M., and Hoflack, B. (2012) Bridging membrane and cytoskeleton dynamics in the secretory and endocytic pathways. *Nat. Cell Biol.* **14,** 11–19
35. Willenborg, C., Jing, J., Wu, C., Matern, H., Schaack, J., Burden, J., and Prekeris, R. (2011) Interaction between FIP5 and SNX18 regulates epithelial lumen formation. *J. Cell Biol.* **195,** 71–86
36. Sancho, E., Batlle, E., and Clevers, H. (2003) Live and let die in the intestinal epithelium. *Curr. Opin. Cell Biol.* **15,** 763–770
37. Coskun, U., and Simons, K. (2010) Membrane rafting. From apical sorting to phase segregation. *FEBS Lett.* **584,** 1685–1693
38. Elkjaer, M. L., Nejsum, L. N., Gresz, V., Kwon, T. H., Jensen, U. B., Frøkiaer, J., and Nielsen, S. (2001) Immunolocalization of aquaporin-8 in rat kidney, gastrointestinal tract, testis, and airways. *Am. J. Physiol. Renal Physiol.* **281,** F1047–F1057
39. Iqbal, J., and Hussain, M. M. (2009) Intestinal lipid absorption. *Am. J. Physiol. Endocrinol. Metab.* **296,** E1183–E1194
40. Mansbach, C. M., 2nd, and Gorelick, F. (2007) Development and physiological regulation of intestinal lipid absorption. II. Dietary lipid absorption, complex lipid synthesis, and the intracellular packaging and secretion of chylomicrons. *Am. J. Physiol. Gastrointest. Liver Physiol.* **293,** G645–G650
41. Tso, P., Nauli, A., and Lo, C. M. (2004) Enterocyte fatty acid uptake and intestinal fatty acid-binding protein. *Biochem. Soc. Trans.* **32,** 75–78
42. Hansen, G. H., Niels-Christiansen, L. L., Immerdal, L., Nystrøm, B. T., and Danielsen, E. M. (2007) Intestinal alkaline phosphatase. Selective endocytosis from the enterocyte brush border during fat absorption. *Am. J. Physiol. Gastrointest. Liver Physiol.* **293,** G1325–G1332
43. Cheng, Z. J., Singh, R. D., Sharma, D. K., Holicky, E. L., Hanada, K., Marks, D. L., and Pagano, R. E. (2006) Distinct mechanisms of clathrin-independent endocytosis have unique sphingolipid requirements. *Mol. Biol. Cell* **17,** 3197–3210
44. Ghidoni, R., Trinchera, M., Venerando, B., Fiorilli, A., Sonnino, S., and Tettamanti, G. (1986) Incorporation and metabolism of exogenous GM1 ganglioside in rat liver. *Biochem. J.* **237,** 147–155
45. Riboni, L., Bassi, R., Sonnino, S., and Tettamanti, G. (1992) Formation of free sphingosine and ceramide from exogenous ganglioside GM1 by cerebellar granule cells in culture. *FEBS Lett.* **300,** 188–192
46. Riboni, L., Prinetti, A., Pitto, M., and Tettamanti, G. (1990) Patterns of endogenous gangliosides and metabolic processing of exogenous gangliosides in cerebellar granule cells during differentiation in culture. *Neurochem. Res.* **15,** 1175–1183
47. Chigorno, V., Giannotta, C., Ottico, E., Sciannamblo, M., Mikulak, J., Prinetti, A., and Sonnino, S. (2005) Sphingolipid uptake by cultured cells. Complex aggregates of cell sphingolipids with serum proteins and lipoproteins are rapidly catabolized. *J. Biol. Chem.* **280,** 2668–2675